

**PARTIAL RELAXATION OF C^0 VERTEX CONTINUITY OF STRESSES OF
CONFORMING MIXED FINITE ELEMENTS FOR THE ELASTICITY
PROBLEM**

JUN HU AND RUI MA

ABSTRACT. A conforming triangular mixed element recently proposed by Hu and Zhang for linear elasticity is extended by rearranging the global degrees of freedom. More precisely, adaptive meshes $\mathcal{T}_1, \dots, \mathcal{T}_N$ which are successively refined from an initial mesh \mathcal{T}_0 through a newest vertex bisection strategy, admit a crucial hierarchical structure, namely, a newly added vertex \mathbf{x}_e of the mesh \mathcal{T}_ℓ is the midpoint of an edge e of the coarse mesh $\mathcal{T}_{\ell-1}$. Such a hierarchical structure is explored to partially relax the C^0 vertex continuity of symmetric matrix-valued functions in the discrete stress space of the original element on \mathcal{T}_ℓ and results in an extended discrete stress space: for such an internal vertex \mathbf{x}_e located at the coarse edge e with the unit tangential vector t_e and the unit normal vector $n_e = t_e^\perp$, the pure tangential component basis function $\varphi_{\mathbf{x}_e}(\mathbf{x})t_e t_e^T$ of the original discrete stress space associated to vertex \mathbf{x}_e is split into two basis functions $\varphi_{\mathbf{x}_e}^+(\mathbf{x})t_e t_e^T$ and $\varphi_{\mathbf{x}_e}^-(\mathbf{x})t_e t_e^T$ along edge e , where $\varphi_{\mathbf{x}_e}(\mathbf{x})$ is the nodal basis function of the scalar-valued Lagrange element of order k (k is equal to the polynomial degree of the discrete stress) on \mathcal{T}_ℓ with $\varphi_{\mathbf{x}_e}^+(\mathbf{x})$ and $\varphi_{\mathbf{x}_e}^-(\mathbf{x})$ denoted its two restrictions on two sides of e , respectively. Since the remaining two basis functions $\varphi_{\mathbf{x}_e}(\mathbf{x})n_e n_e^T$, $\varphi_{\mathbf{x}_e}(\mathbf{x})(n_e t_e^T + t_e n_e^T)$ are the same as those associated to \mathbf{x}_e of the original discrete stress space, the number of the global basis functions associated to \mathbf{x}_e of the extended discrete stress space becomes four rather than three (for the original discrete stress space). As a result, though the extended discrete stress space on \mathcal{T}_ℓ is still a $H(\text{div})$ subspace, the pure tangential component along the coarse edge e of discrete stresses in it is not necessarily continuous at such vertices like \mathbf{x}_e . A feature of this extended discrete stress space is its nestedness in the sense that a space on a coarse mesh \mathcal{T} is a subspace of a space on any refinement $\hat{\mathcal{T}}$ of \mathcal{T} , which allows a proof of convergence of a standard adaptive algorithm. The idea is extended to impose a general traction boundary condition on the discrete level. Numerical experiments are provided to illustrate performance on both uniform and adaptive meshes.

Keywords. linear elasticity, nested mixed finite element, adaptive algorithm

AMS subject classifications. 65N30, 74B05.

1. INTRODUCTION

The problems that are most frequently solved in scientific and engineering computing may probably be elasticity equations. The finite element method (FEM) was invented in analyzing the stress of elastic structures in the 1950s. The mixed FEM within the Hellinger-Reissner (H-R) principle for elasticity yields a direct stress approximation since it takes both the stress and displacement as an independent variable; while the displacement FEM only gives an indirect stress approximation. Hu, a founder of the celebrated Hu-Washizu

The authors were supported by NSFC projects 11625101 and 11421101.

principle for elasticity, pointed out that, the H-R principle is more general than both minimum potential and complementary energy principles, and is much fitter for numerical solutions [20]. Indeed, the mixed FEM can be free of locking for nearly incompressible materials, and be applied to plastic materials, and approximate both equilibrium and traction boundary conditions more accurate. However, symmetry of the stress and stability of the mixed FEM make the design of the mixed FEM for elasticity surprisingly hard, which has been regarded as a long standing open problem [3]. In fact, "Four decades of searching for mixed finite elements for elasticity beginning in the 1960s did not yield any stable elements with polynomial shape functions" [D. N. Arnold, Proceedings of the ICM, Vol. I : Plenary Lectures and Ceremonies (2002)].

Since the 1960s, many mathematicians have worked on this problem but compromised to weakly symmetric elements [4, 5, 8], or composite elements [29]. In 2002, using the elasticity complexes, Arnold and Winther designed the first family of symmetric mixed elements with polynomial shape functions on triangular grids in 2D [6] which was extended to tetrahedral grids in 3D [3] (see also [1] for the first order element in three dimensions) and to rectangular grids in 2D [2]. Recently, the first author and his collaborators developed a new framework to design and analyze the mixed FEM of elasticity equations, which yields a family of optimal symmetric mixed FEMs. In addition, those elements are very easy to implement since their basis functions, based on those of the scalar-valued Lagrange elements, can be explicitly written down by hand. The main ingredients of this framework are a structure of the discrete stress space on both simplicial and product grids, two basic algebraic results, and a two-step stability analysis method, see more details in [21, 22, 24, 25, 26].

However, due to the constraint of symmetry, all the aforementioned symmetric conforming mixed elements on triangular meshes impose C^0 continuity of discrete stresses at internal vertices. Such C^0 vertex continuity causes the failure of nestedness. In fact, for an admissible mesh $\hat{\mathcal{T}}$ which is refined from a coarse mesh \mathcal{T} , a newly added internal vertex x_e of $\hat{\mathcal{T}}$ is a midpoint of a coarse edge e of \mathcal{T} with the unit tangential and normal vectors t_e and $n_e = t_e^\perp$, respectively. All the components of a symmetric matrix-valued function in the discrete stress space $\Sigma(\hat{\mathcal{T}})$ on $\hat{\mathcal{T}}$ are continuous at the aforementioned vertex x_e . Whereas for a symmetric matrix-valued function τ in the discrete stress space $\Sigma(\mathcal{T})$ on \mathcal{T} , two components $n_e^T \tau n_e$ and $t_e^T \tau n_e$ are continuous while the pure tangential component $t_e^T \tau t_e$ is not necessarily continuous at this vertex. This is to say τ is not necessarily in the fine space $\Sigma(\hat{\mathcal{T}})$ and consequently $\Sigma(\mathcal{T})$ is not a subspace of $\Sigma(\hat{\mathcal{T}})$. Thus there is no nestedness.

There are plenty of results about the convergence analysis of adaptive mixed FEMs for the mixed Poisson problem [7, 10, 14, 17, 23, 28] and [27] for Kirchhoff plate bending problems. These results are established for nested finite element spaces on adaptive meshes. The non-nestedness of the discrete stress space of the elements of [1, 3, 6, 21, 22, 24, 25, 26] leads to mathematical difficulty of their adaptive algorithms, based on a posteriori error estimators of the two families of triangular mixed elements, see [11, 12, 18]. In fact, for the convergence analysis of standard adaptive algorithms of non-nested conforming methods including mixed methods, the only positive result is the paper [31] where the non-nestedness is caused by a very particular mesh-refinement strategy, while the non-nestedness herein comes from extra continuity of functions at the internal vertices in the discrete stress space. It is unclear for the authors whether the technology of [31] can be extended to the current case.

One purpose of this paper is to extend a conforming triangular mixed element recently proposed in [21, 24] by Hu and Zhang for linear elasticity by rearranging the global degrees

of freedom. The underlying admissible meshes $\mathcal{T}_1, \dots, \mathcal{T}_N$ are successively refined from an initial mesh \mathcal{T}_0 through a newest vertex bisection strategy [30]. It has already been explained that these meshes admit a crucial hierarchical structure, namely, a newly added vertex x_e of the mesh \mathcal{T}_ℓ is the midpoint of an edge e of the coarse mesh $\mathcal{T}_{\ell-1}$. Such a hierarchical structure will be explored to partially relax C^0 vertex continuity of symmetric matrix-valued functions in the discrete stress space $\Sigma(\mathcal{T}_\ell)$ on \mathcal{T}_ℓ of the original element and results in an extended discrete stress space $\widetilde{\Sigma}(\mathcal{T}_\ell)$. For such an internal vertex x_e located at the coarse edge e with the unit tangential vector t_e and the unit normal vector $n_e = t_e^\perp$, let $\varphi_{x_e}(\mathbf{x})$ be the nodal basis function of the scalar-valued Lagrange element of order k (k is equal to the polynomial degree of the discrete stress) on \mathcal{T}_ℓ with $\varphi_{x_e}^+(\mathbf{x})$ and $\varphi_{x_e}^-(\mathbf{x})$ denoted its two restrictions on two sides of e , respectively. The idea to extend $\Sigma(\mathcal{T}_\ell)$ is to keep the continuity of the normal components τn_e of a symmetric matrix-valued function τ in $\Sigma(\mathcal{T}_\ell)$ and to split the pure tangential component $t_e^T \tau t_e$ into two parts at vertex x_e along edge e . This can be accomplished by splitting the basis function $\varphi_{x_e}(\mathbf{x}) t_e t_e^T$ into two basis functions $\varphi_{x_e}^+(\mathbf{x}) t_e t_e^T$ and $\varphi_{x_e}^-(\mathbf{x}) t_e t_e^T$ while keeping the other two basis functions $\varphi_{x_e}(\mathbf{x}) n_e n_e^T$ and $\varphi_{x_e}(\mathbf{x}) (n_e t_e^T + t_e n_e^T)$, associated to vertex x_e . This is, though the extended discrete stress space $\widetilde{\Sigma}(\mathcal{T}_\ell)$ on \mathcal{T}_ℓ is still a $H(\text{div})$ subspace, the pure tangential component along the coarse edge e of discrete stresses in it is not necessarily continuous at such vertices like x_e . Therefore, the number of the global basis functions associated to the node x_e of the extended discrete stress space becomes four rather than three (for the original discrete stress space). A feature of this extended discrete stress space is its nestedness in the sense that the space $\widetilde{\Sigma}(\mathcal{T}_{\ell-1})$ is a subspace of $\widetilde{\Sigma}(\mathcal{T}_\ell)$. Then, such a nested property is used to analyze and prove the optimal convergence of a standard adaptive algorithm.

Another purpose of the paper is to impose a general traction boundary condition on the discrete level. The underlying situation is that a corner x_c of the polygonal domain Ω is the unique intersected point of two boundary edges e_1 and e_2 . Let t_i and n_i denote the unit tangential and outward normal vectors of e_i , $i = 1, 2$. A general traction boundary condition $\sigma n_i|_{e_i}$, $i = 1, 2$, imposed on both e_1 and e_2 can be inconsistent (discontinuous) in the sense that $n_2^T \sigma n_1|_{e_1}(x_c) \neq n_1^T \sigma n_2|_{e_2}(x_c)$. Such inconsistency (discontinuity) causes an essential difficulty for imposing such a boundary condition if the vertex degrees of freedom of the original discrete stress space are used at the corner vertex x_c . Indeed, it holds that $n_2^T \tau n_1|_{e_1}(x_c) = n_1^T \tau n_2|_{e_2}(x_c)$ for any τ in $\Sigma(\mathcal{T})$ on the mesh \mathcal{T} for all the elements in [6, 21, 24]. As a result, the traction boundary condition can not be exactly imposed even if $\sigma n_i|_{e_i}$ is a polynomial of degree not bigger than k if $n_2^T \sigma n_1|_{e_1}(x_c) \neq n_1^T \sigma n_2|_{e_2}(x_c)$. To handle such a case, the authors of [13] compromised to a least square method to obtain some approximation of the traction boundary condition. The idea to overcome such a difficulty is to split the triangle at the corner into two sub-triangles and then relax the continuity of the pure tangential component across the common edge of these two sub-triangles. This eventually leads to four degrees of freedom at the corner vertex. As a result, the possible inconsistent traction boundary condition is able to be imposed, in particular, be exactly imposed if $\sigma n_i|_{e_i}$ is a polynomial of degree not bigger than k . The numerical results on uniform meshes and adaptive meshes for a benchmark problem over an L-shaped domain and Cook's membrane problem indicate that such a remedy is able to largely improve accuracy of discrete stresses especially on coarse meshes. The reason lies in that the error caused by the inexact boundary conditions may dominate on coarse meshes.

Throughout this paper, $L^2(\omega; X)$ denotes the space of functions which are square-integrable with domain ω . For our purposes, the range space X will be either $\mathbb{S} := \text{symmetric } \mathbb{R}^{d \times d}$, \mathbb{R}^d , or \mathbb{R} , $d = 2, 3$. Let $H^m(\omega; X)$ denote the Sobolev space consisting of functions, taking

values in the finite-dimensional vector space X , and with all derivatives of order at most m square-integrable, and $H(\text{div}, \omega; \mathbb{S})$ consist of square-integrable symmetric matrix fields with square-integrable divergence. Let $\|\cdot\|_{m,\omega}$ represent the norm and $|\cdot|_{m,\omega}$ represent the seminorm of $H^m(\omega)$, and $(\cdot, \cdot)_\omega$ represent as usual, the L^2 inner product on the domain ω , the subscript ω is omitted when $\omega = \Omega$. $\langle \cdot, \cdot \rangle_\Gamma$ represents the L^2 inner product on the boundary Γ . For $\phi \in H^1(\Omega; \mathbb{R})$, $v = (v_1, v_2)^T \in H^1(\Omega; \mathbb{R}^2)$, set

$$\text{Curl}\phi := (-\partial\phi/\partial x_2, \partial\phi/\partial x_1), \quad \text{Curl}v := \begin{pmatrix} -\partial v_1/\partial x_2 & \partial v_1/\partial x_1 \\ -\partial v_2/\partial x_2 & \partial v_2/\partial x_1 \end{pmatrix}.$$

For $v = (v_1, v_2)^T \in H^1(\Omega; \mathbb{R}^2)$ and $\tau = (\tau_{ij})_{2 \times 2}$, set

$$\text{curl}v := \partial v_2/\partial x_1 - \partial v_1/\partial x_2, \quad \text{curl}\tau = \begin{pmatrix} \partial\tau_{12}/\partial x_1 - \partial\tau_{11}/\partial x_2 \\ \partial\tau_{22}/\partial x_1 - \partial\tau_{21}/\partial x_2 \end{pmatrix}.$$

The notation $A \lesssim B$ abbreviates $A \leq CB$ for a mesh-size independent constant $C > 0$. The context depending symbol $|\bullet|$ denotes the area of a domain, the length of a edge, the counting measure (cardinality) of a set and the absolute value of a real number.

The rest of the paper is organized as follows. Section 2 introduces notation in this paper and the mixed element on triangular meshes [21, 24], including its degrees of freedom and basis functions. Section 3 designs nested mixed finite elements on adaptive meshes by partially relaxing the C^0 vertex continuity of discrete stresses at newly added internal vertices of refined meshes and proves optimality of the corresponding adaptive algorithm. In Section 4, the C^0 vertex continuity is relaxed at corner vertices of domain Ω so that an inconsistent traction boundary condition on Γ_N can be imposed. This section will give some comments to the three dimensional case. Numerical experiments are presented in Section 5.

2. PRELIMINARIES

This section introduces the stress-displacement formulation for linear elasticity and the mixed FEM from [21, 24].

2.1. Mixed formulation. Let $\Omega \subset \mathbb{R}^2$ be a simply-connected bounded polygonal domain with boundary $\Gamma := \partial\Omega = \Gamma_D \cup \Gamma_N$, $\Gamma_D \cap \Gamma_N = \emptyset$. Given $f \in V := L^2(\Omega; \mathbb{R}^2)$, $u_D \in H^1(\Omega; \mathbb{R}^2)$ and $g \in L^2(\Gamma_N; \mathbb{R}^2)$, the linear elasticity problem with mixed boundary conditions within a stress-displacement formulation reads: Seek $(\sigma, u) \in \Sigma_g \times V$ such that

$$(2.1) \quad \begin{cases} (A\sigma, \tau) + (\text{div}\tau, u) = \langle u_D, \tau n \rangle_{\Gamma_D} & \text{for all } \tau \in \Sigma_0, \\ (\text{div}\sigma, v) = (f, v) & \text{for all } v \in V \end{cases}$$

with

$$W := \{v \in H^1(\Omega; \mathbb{R}^2) \mid v|_{\Gamma_D} = 0\},$$

$$\Sigma_g := \{\sigma \in H(\text{div}, \Omega; \mathbb{S}) \mid \langle \psi, \sigma n \rangle_{\Gamma_N} = \langle \psi, g \rangle_{\Gamma_N} \text{ for all } \psi \in W\}.$$

Here $\Sigma_0 := \Sigma_g$ with $g \equiv 0$ and n denotes the outnormal of $\partial\Omega$. The compliance tensor $A : \mathbb{S} \rightarrow \mathbb{S}$, characterizing the properties of the material, is symmetric positive definite and its eigenvalues are uniformly bounded from above. In the homogeneous isotropic case, the compliance tensor is given by $A\tau = (\tau - \lambda/(2\mu + 2\lambda)\text{tr}\tau\mathbf{I})/(2\mu)$ with the Lamé constants $\mu > 0$ and $\lambda \geq 0$, the identity matrix \mathbf{I} and the trace $\text{tr}\tau$ of the matrix τ . For simplicity, this paper assumes A is a constant tensor.

2.2. Triangulations. Given an initial shape-regular triangulation \mathcal{T}_0 of Ω into triangles, let $\mathbb{T} := \mathbb{T}(\mathcal{T}_0)$ denote the set of all admissible regular triangulations obtained from \mathcal{T}_0 with a finite number of successive bisections of triangles by the newest vertex bisection [30]. Given $\mathcal{T} \in \mathbb{T}$, let $\hat{\mathcal{T}}$ denote a refinement of \mathcal{T} , and $\mathcal{T} \setminus \hat{\mathcal{T}} := \{K \in \mathcal{T} \mid K \notin \hat{\mathcal{T}}\}$ denote the set of refined elements from \mathcal{T} to $\hat{\mathcal{T}}$. Let $h_K := |K|^{1/2}$ and $h = \max_{K \in \hat{\mathcal{T}}} h_K$. Denote by $\hat{\mathcal{E}}$ (resp. $\hat{\mathcal{E}}(\Omega)$ and $\hat{\mathcal{E}}(\Gamma)$) the collection of all (resp. interior and boundary) element edges of $\hat{\mathcal{T}}$. For any triangle $K \in \hat{\mathcal{T}}$, let $\mathcal{E}(K)$ denote the set of its edges. For any edge $e \in \hat{\mathcal{E}}$, let t_e denote the unit tangential vector and let $n_e := t_e^\perp$ denote the unit normal vector. If $e \in \hat{\mathcal{E}}(\Gamma)$, $n_e = n$ is the outward unit normal. The jump $[w]_e$ of w across edge $e = K_1 \cap K_2$ reads

$$[w]_e := (w|_{K_1})|_e - (w|_{K_2})|_e.$$

Particularly, if $e \in \hat{\mathcal{E}}(\Gamma)$, $[w]_e := w|_e$. Let $\mathcal{V}(\hat{\mathcal{T}})$ (resp. $\mathcal{V}_0(\hat{\mathcal{T}})$) denote the set of all (resp. internal) vertices of $\hat{\mathcal{T}}$. The newest-vertex bisection (NVB) (see more details in [30]) creates each new vertex $x_e \in \mathcal{V}(\hat{\mathcal{T}}) \setminus \mathcal{V}(\mathcal{T}_0)$ as a midpoint of some edge e associated with tangential vector t_e and normal vector n_e . Given any internal node $x_e \in \mathcal{V}_0(\hat{\mathcal{T}}) \setminus \mathcal{V}(\mathcal{T}_0)$, define the two patches $\omega_{x_e}^+$ and $\omega_{x_e}^-$ by

$$(2.2) \quad \begin{aligned} \omega_{x_e}^+ &:= \cup\{K \mid K \in \hat{\mathcal{T}}, x_e \in K, (\text{mid}(K) - x_e) \cdot n_e > 0\}, \\ \omega_{x_e}^- &:= \cup\{K \mid K \in \hat{\mathcal{T}}, x_e \in K, (\text{mid}(K) - x_e) \cdot n_e < 0\}. \end{aligned}$$

Given any integer $k \geq 0$, let $P_k(\omega; X)$ denote the space of polynomials over ω of total degree not greater than k , taking values in the finite-dimensional vector space X . Let x_i , $1 \leq i \leq 3$ denote the vertices of $K \in \hat{\mathcal{T}}$, λ_i denote the barycentric coordinates with respect to x_i , and $t_{i,j} = x_j - x_i$ denote the tangential vector of edge $x_i x_j$.

2.3. Mixed finite element method. Given $K \in \hat{\mathcal{T}}$, with symmetric matrices $\mathbb{S}_{i,j} := t_{i,j} t_{i,j}^T$, $1 \leq i < j \leq 3$ of rank one, define the following space [21, 24]:

$$\Sigma_{k,b}(K) := \sum_{1 \leq i < j \leq 3} \lambda_i \lambda_j P_{k-2}(K; \mathbb{R}) \mathbb{S}_{i,j}.$$

Note that for any function $\tau \in \Sigma_{k,b}(K)$ and any edge e of K with the normal vector n_e , the normal components $\tau n_e|_e$ vanish. This is to say $\Sigma_{k,b}(K)$ is an $H(\text{div}, K; \mathbb{S})$ bubble function space on K . With such a bubble function space on each element of $\hat{\mathcal{T}}$, one can define a discrete stress space $\Sigma(\hat{\mathcal{T}})$ with a simple and crucial structure on $\hat{\mathcal{T}}$, i.e., for $k \geq 3$,

$$(2.3) \quad \begin{aligned} \Sigma(\hat{\mathcal{T}}) &:= \{\sigma \in H(\text{div}, \Omega; \mathbb{S}) \mid \sigma = \sigma_c + \sigma_b, \sigma_c \in H^1(\Omega; \mathbb{S}), \\ &\quad \forall K \in \hat{\mathcal{T}}, \sigma_c|_K \in P_k(K; \mathbb{S}), \sigma_b|_K \in \Sigma_{k,b}(K)\}. \end{aligned}$$

Note that σ_c is a symmetric matrix-valued H^1 Lagrange element function, this is, each component of σ_c is a scalar-valued Lagrange element function on $\hat{\mathcal{T}}$. This is, the discrete stress space $\Sigma(\hat{\mathcal{T}})$ is a sum of the symmetric matrix-valued H^1 Lagrange element function space and these $H(\text{div})$ bubble function spaces. While the bubble function space $\Sigma_{k,b}(K)$ on element K plays a very important role in the two step stability analysis of the element, see [21, 24] for more details.

Next, the degrees of freedom will be presented for the stress shape function space $P_k(K; \mathbb{S})$ on element K . Indeed, a symmetric matrix field $\tau \in P_k(K; \mathbb{S})$ can be uniquely determined by the degrees of freedom from (1), (2) and (3) (see Figure 2.1 with solid points and arrows for $k = 3$) [21]:

- (1) the values of τ at three vertices,
- (2) for edge e , the mean moments of degree at most $k - 2$ over e of $n_e \tau n_e^T$, $t_e^T \tau n_e$,

(3) the values $\int_K \tau : \xi dx$ for any $\xi \in \Sigma_{k,b}(K)$.

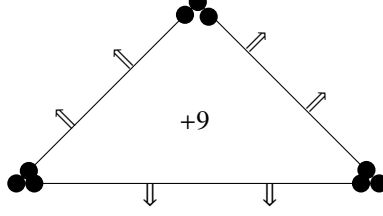


FIGURE 2.1. Degrees of freedom for $\Sigma(\hat{\mathcal{T}})$ of $k = 3$

For ease implementation, the global basis functions of $\Sigma(\hat{\mathcal{T}})$ when $k = 3$ will be presented, which needs the nodal basis functions of the scalar-valued Lagrange element of order 3, which, on element K , read as follows

$$\begin{aligned}\varphi_0(\mathbf{x}) &= 27\lambda_1\lambda_2\lambda_3, \\ \varphi_i(\mathbf{x}) &= \frac{9}{2}\lambda_i(\lambda_i - \frac{1}{3})(\lambda_i - \frac{2}{3}), i = 1, 2, 3, \\ \varphi_{ij}(\mathbf{x}) &= \frac{27}{2}\lambda_{i+1}\lambda_{i+2}(\lambda_{i+j} - \frac{1}{3}), i = 1, 2, 3, j = 1, 2.\end{aligned}$$

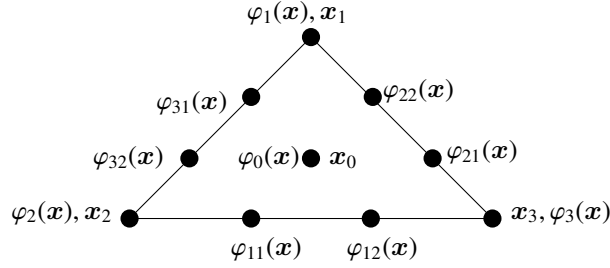


FIGURE 2.2. Ten nodal basis functions of the Lagrange element of order 3 on element K .

Two sets of basis of the symmetric matrix space \mathbb{S} are required as well. The first set of basis is the canonical basis of \mathbb{S} :

$$(2.4) \quad \mathbb{S}_1 = \begin{pmatrix} 1 & 0 \\ 0 & 0 \end{pmatrix}, \mathbb{S}_2 = \begin{pmatrix} 0 & 1 \\ 1 & 0 \end{pmatrix}, \text{ and } \mathbb{S}_3 = \begin{pmatrix} 0 & 0 \\ 0 & 1 \end{pmatrix}.$$

The second set of basis of \mathbb{S} is defined associated to each edge. More precisely, given edge e_i of element K , define $\mathbb{S}_{e_i} := t_{e_i}t_{e_i}^T$ and $\mathbb{S}_{e_i,m}^\perp$ with $m = 1, 2$ such that

$$(2.5) \quad \mathbb{S}_{e_i,1}^\perp := n_{e_i}n_{e_i}^T, \mathbb{S}_{e_i,2}^\perp := n_{e_i}t_{e_i}^T + t_{e_i}n_{e_i}^T, \text{ therefore, } \mathbb{S}_{e_i,m}^\perp : \mathbb{S}_{e_i} = 0 \text{ and } \mathbb{S}_{e_i,1}^\perp : \mathbb{S}_{e_i,2}^\perp = 0.$$

Then, the global basis functions of the discrete stress space associated to element K are as follows:

$$(2.6) \quad \begin{aligned}\theta_{ij} &= \varphi_i(\mathbf{x})\mathbb{S}_j, i = 0, 1, 2, 3, j = 1, 2, 3, \\ \alpha_{ij} &= \varphi_{ij}(\mathbf{x})|_K \mathbb{S}_{e_i}, i = 1, 2, 3, j = 1, 2, \\ \beta_{ijm} &= \varphi_{ij}(\mathbf{x})\mathbb{S}_{e_i,m}^\perp, i = 1, 2, 3, j = 1, 2, m = 1, 2.\end{aligned}$$

Here $\varphi_{ij}(\mathbf{x})|_K$ denotes the restriction of $\varphi_{ij}(\mathbf{x})$ on element K . Note that the basis function α_{ij} is an $H(\text{div})$ bubble function in the sense that $\alpha_{ij}n_e|_e = 0$ on any edge e of element K . Furthermore, if e_i is a common edge of element K and element K' , the corresponding $H(\text{div})$ bubble function with respect to element K' is $\alpha'_{ij} = \varphi_{ij}(\mathbf{x})|_{K'}\mathbb{S}_{e_i}$ which is also a basis function of $\Sigma(\hat{\mathcal{T}})$ and independent of α_{ij} . It is stressed that a basis function of $\Sigma(\hat{\mathcal{T}})$ is the product of a scalar-valued Lagrange element basis function (or the corresponding restriction on an element) and a basis of the symmetric matrix space \mathbb{S} .

The displacement space is the full C^{-1} - P_{k-1} space

$$(2.7) \quad V(\hat{\mathcal{T}}) := \{v \in L^2(\Omega; \mathbb{R}^2) \mid v|_K \in P_{k-1}(K; \mathbb{R}^2) \text{ for all } K \in \hat{\mathcal{T}}\}.$$

Suppose $g(\hat{\mathcal{T}}) := \alpha(\hat{\mathcal{T}})n|_{\Gamma_N}$ for some $\alpha(\hat{\mathcal{T}}) \in \Sigma(\hat{\mathcal{T}})$ denotes some approximation to g . The mixed FEM to (2.1) seeks $(\sigma(\hat{\mathcal{T}}), u(\hat{\mathcal{T}})) \in \Sigma(\hat{\mathcal{T}}) \cap \Sigma_{g(\hat{\mathcal{T}})} \times V(\hat{\mathcal{T}})$ such that

$$(2.8) \quad \begin{cases} (A\sigma(\hat{\mathcal{T}}), \tau(\hat{\mathcal{T}})) + (\text{div}\tau(\hat{\mathcal{T}}), u(\hat{\mathcal{T}})) = \langle u_D, \tau(\hat{\mathcal{T}})n \rangle_{\Gamma_D} & \text{for all } \tau(\hat{\mathcal{T}}) \in \Sigma(\hat{\mathcal{T}}) \cap \Sigma_0, \\ (\text{div}\sigma(\hat{\mathcal{T}}), v(\hat{\mathcal{T}})) = (f, v(\hat{\mathcal{T}})) & \text{for all } v(\hat{\mathcal{T}}) \in V(\hat{\mathcal{T}}). \end{cases}$$

3. ADAPTIVE MIXED FINITE ELEMENT METHODS

Due to the vertex C^0 continuity of functions in $\Sigma(\hat{\mathcal{T}})$ from (2.3), as it was explained in the introduction that the discrete stress space is non-nested in the sense that a coarse space $\Sigma(\mathcal{T})$ is not a subspace of a fine space $\Sigma(\hat{\mathcal{T}})$ when $\hat{\mathcal{T}}$ is an admissible refinement of \mathcal{T} by NVB. In fact, a newly added internal vertex x_e of $\hat{\mathcal{T}}$ is a midpoint of an coarse edge e of \mathcal{T} with the unit tangential and normal vectors t_e and $n_e = t_e^\perp$, respectively. The vertex C^0 continuity implies that all the components of functions in $\Sigma(\hat{\mathcal{T}})$ are continuous at vertex x_e . However, for a function τ in $\Sigma(\mathcal{T})$, its pure tangential component $t_e^T \tau t_e$ is not necessarily continuous at this vertex. This is to say τ is not necessarily in the fine space $\Sigma(\hat{\mathcal{T}})$ and consequently $\Sigma(\mathcal{T})$ is not a subspace of $\Sigma(\hat{\mathcal{T}})$. With such non-nestedness, it is actually very difficult to analyze the optimal convergence of the corresponding adaptive algorithm. In the adaptive algorithm, the underlying admissible meshes $\mathcal{T}_1, \dots, \mathcal{T}_N$, based on some a posteriori error estimate, see for instance [18], are successively refined from an initial mesh \mathcal{T}_0 through a NVB strategy [30]. Since $\Sigma(\mathcal{T}_\ell)$ is usually not a subspace of $\Sigma(\mathcal{T}_m)$ with $m > \ell$, it is essentially difficult to show some orthogonality or quasi-orthogonality which is a main ingredient for the optimal convergence analysis of adaptive algorithms [10, 23]. For the non-nestedness caused by the extra smoothness of the underlying finite element space, there is no convergence analysis of the corresponding adaptive algorithm in the literature so far.

This section relaxes the C^0 vertex continuity of functions in $\Sigma(\hat{\mathcal{T}})$ to design an extended stress space $\widetilde{\Sigma}(\hat{\mathcal{T}})$ when $\hat{\mathcal{T}}$ is a refinement of \mathcal{T} by NVB. For the admissible nested meshes $\mathcal{T}_0, \mathcal{T}_1, \dots, \mathcal{T}_N$ from the adaptive algorithm, this leads to a sequence of nested spaces $\Sigma(\mathcal{T}_0), \widetilde{\Sigma}(\mathcal{T}_1), \dots, \widetilde{\Sigma}(\mathcal{T}_N)$. The optimal convergence of the adaptive algorithm based on these nested spaces will be proved, adopted to the unified analysis from [23]. For simplicity, this section only considers the homogeneous Dirichlet boundary condition $\Gamma_D = \Gamma$ and $u_D \equiv 0$.

3.1. Extended stress space on adaptive meshes. The extended stress space $\widetilde{\Sigma}(\hat{\mathcal{T}})$ extends the global degrees of freedom (1) of $\Sigma(\hat{\mathcal{T}})$ from Subset. 2.3 to make it hierarchical and defined for an admissible triangulation $\hat{\mathcal{T}} \in \mathbb{T}$ as follows. Recall that any internal vertex $x_e \in \mathcal{V}_0(\hat{\mathcal{T}}) \setminus \mathcal{V}(\mathcal{T}_0)$ (e is a coarse edge and x_e is its midpoint) is associated to the separation $\omega_{x_e}^+$ and $\omega_{x_e}^-$ of the neighbouring triangles with vertex x_e . Instead of the continuity

of all components of τ at x_e , the component $t_e^T \tau t_e$ at x_e is not uniquely defined at x_e but allows for one value in $\omega_{x_e}^+$ and a second value in $\omega_{x_e}^-$. Meanwhile, the vertex-based basis functions associated to x_e are enriched to four basis functions:

$$(3.1) \quad \varphi_{x_e}(\mathbf{x})n_e n_e^T, \varphi_{x_e}(\mathbf{x})(n_e t_e^T + t_e n_e^T), \tau_{x_e}^+ := \varphi_{x_e}^+(\mathbf{x})t_e t_e^T \text{ and } \tau_{x_e}^- := \varphi_{x_e}^-(\mathbf{x})t_e t_e^T.$$

Here $\varphi_{x_e}^+(\mathbf{x}) = \varphi_{x_e}(\mathbf{x})$ for $\mathbf{x} \in \omega_{x_e}^+$ and otherwise vanishes, and $\varphi_{x_e}^-(\mathbf{x})$ is similarly defined for $\omega_{x_e}^-$.

Let $E(\hat{\mathcal{T}}) := \text{span}_{\mathbf{x}_e \in \mathcal{V}_0(\hat{\mathcal{T}}) \setminus \mathcal{V}(\mathcal{T}_0)} \{\tau_{x_e}^+, \tau_{x_e}^-\}$. The extended stress space is then defined by

$$(3.2) \quad \widetilde{\Sigma}(\hat{\mathcal{T}}) := \Sigma(\hat{\mathcal{T}}) + E(\hat{\mathcal{T}}).$$

Note that for any $\tau(\hat{\mathcal{T}}) \in E(\hat{\mathcal{T}})$ and any $e \in \hat{\mathcal{E}}(\Omega)$, the normal components $\tau(\hat{\mathcal{T}})n_e$ are continuous across e . This guarantees $E(\hat{\mathcal{T}}) \subset H(\text{div}, \Omega; \mathbb{S})$ and thus $\widetilde{\Sigma}(\hat{\mathcal{T}}) \subset H(\text{div}, \Omega; \mathbb{S})$. The displacement is approximated by $V(\hat{\mathcal{T}})$ in (2.7). Then the extended mixed FEM to (2.1) with homogeneous Dirichlet boundary condition seeks $(\sigma(\hat{\mathcal{T}}), u(\hat{\mathcal{T}})) \in \widetilde{\Sigma}(\hat{\mathcal{T}}) \times V(\hat{\mathcal{T}})$ such that

$$(3.3) \quad \begin{cases} (A\sigma(\hat{\mathcal{T}}), \tau(\hat{\mathcal{T}})) + (\text{div}\tau(\hat{\mathcal{T}}), u(\hat{\mathcal{T}})) = 0 & \text{for all } \tau(\hat{\mathcal{T}}) \in \widetilde{\Sigma}(\hat{\mathcal{T}}), \\ (\text{div}\sigma(\hat{\mathcal{T}}), v(\hat{\mathcal{T}})) = (f, v(\hat{\mathcal{T}})) & \text{for all } v(\hat{\mathcal{T}}) \in V(\hat{\mathcal{T}}). \end{cases}$$

For ease of notation, throughout this section let $(\sigma(\hat{\mathcal{T}}), u(\hat{\mathcal{T}})) \in \widetilde{\Sigma}(\hat{\mathcal{T}}) \times V(\hat{\mathcal{T}})$ denote the solution to (3.3) instead of (2.8).

Theorem 3.1. *For $k \geq 3$, the extended discrete problem (3.3) has a unique solution $(\sigma(\hat{\mathcal{T}}), u(\hat{\mathcal{T}})) \in \widetilde{\Sigma}(\hat{\mathcal{T}}) \times V(\hat{\mathcal{T}})$ and the error estimate holds*

$$(3.4) \quad \|\sigma - \sigma(\hat{\mathcal{T}})\|_{H(\text{div})} + \|u - u(\hat{\mathcal{T}})\|_0 \leq Ch^k (\|\sigma\|_{k+1} + \|u\|_k).$$

Proof. The well-posedness and the error estimate of (2.8) can be found in [21, 24]. Since $\text{div}\Sigma(\hat{\mathcal{T}}) = V(\hat{\mathcal{T}})$ and $\text{div}E(\hat{\mathcal{T}}) \subset V(\hat{\mathcal{T}})$ imply $\text{div}\widetilde{\Sigma}(\hat{\mathcal{T}}) = V(\hat{\mathcal{T}})$, the combination with $\Sigma(\hat{\mathcal{T}}) \subset \widetilde{\Sigma}(\hat{\mathcal{T}})$ leads to the well-posedness of (3.3) and its error estimate (3.4) (see e.g. [8, Prop. 5.4.1]). \square

Theorem 3.2 (nestedness). *Given any $\mathcal{T} \in \mathbb{T}$ and its refinement $\hat{\mathcal{T}}$, the extended stress space with respect to \mathcal{T} satisfies $\widetilde{\Sigma}(\hat{\mathcal{T}}) \subset \widetilde{\Sigma}(\mathcal{T})$.*

Proof. Given an interior edge $e \in \mathcal{E}(\Omega)$ with the attached two triangles $K_j \in \mathcal{T}$ for $j = 1, 2$, the bisection of e and K_j leads to four new global degrees of freedom at the midpoint $x_e := \text{mid}(e) \in \mathcal{V}_0(\hat{\mathcal{T}}) \setminus \mathcal{V}(\mathcal{T})$. Given $\tau(\mathcal{T}) \in \widetilde{\Sigma}(\mathcal{T})$, the polynomial $\tau(\mathcal{T})|_{K_j} \in P_k(K_j; \mathbb{S})$ is continuous along e and the normal component is globally continuous at x_e . Consequently, $\tau(\mathcal{T})$ can be represented with the basis functions in (3.1) and the remaining basis functions of $\Sigma(\hat{\mathcal{T}})$ (e.g. (2.6) for $k = 3$). This concludes the proof. \square

3.2. Error estimator and adaptive algorithm. To establish the adaptive algorithm, this paper employs the a posteriori error estimator $\eta^2(\hat{\mathcal{T}}) := \sum_{K \in \hat{\mathcal{T}}} \eta^2(\hat{\mathcal{T}}, K)$ from [18] with

$$(3.5) \quad \eta^2(\hat{\mathcal{T}}, K) := h_K^4 \|\text{curlcurl}(A\sigma(\hat{\mathcal{T}}))\|_{0,K}^2 + \sum_{e \in \mathcal{E}(K)} (h_K \|\mathcal{J}_{e,1}\|_{0,e}^2 + h_K^3 \|\mathcal{J}_{e,2}\|_{0,e}^2)$$

and

$$\mathcal{J}_{e,1} := \begin{cases} \left[(A\sigma(\hat{\mathcal{T}}))_{t_e} \cdot t_e \right]_e & \text{if } e \in \hat{\mathcal{E}}(\Omega), \\ \left((A\sigma(\hat{\mathcal{T}}))_{t_e} \cdot t_e \right) \Big|_e & \text{if } e \in \hat{\mathcal{E}}(\Gamma), \end{cases}$$

$$\mathcal{J}_{e,2} := \begin{cases} \left[\text{curl}(A\sigma(\hat{\mathcal{T}})) \cdot t_e \right]_e & \text{if } e \in \hat{\mathcal{E}}(\Omega), \\ \left(\text{curl}(A\sigma(\hat{\mathcal{T}})) \cdot t_e - \partial_{t_e}((A\sigma(\hat{\mathcal{T}}))_{t_e} \cdot n_e) \right) \Big|_e & \text{if } e \in \hat{\mathcal{E}}(\Gamma). \end{cases}$$

Let $\eta^2(\hat{\mathcal{T}}, \mathcal{M}) := \sum_{K \in \mathcal{M}} \eta^2(\hat{\mathcal{T}}, K)$ for all $\mathcal{M} \subseteq \hat{\mathcal{T}}$. Let $Q_{\hat{\mathcal{T}}}$ denote the L^2 orthogonal projection onto $V(\hat{\mathcal{T}})$. The data oscillation reads

$$\text{osc}^2(f, \mathcal{M}) := \sum_{K \in \mathcal{M}} h_K^2 \|f - Q_{\hat{\mathcal{T}}} f\|_{0,K}^2.$$

Recall the solution (σ, u) to (2.1) with $\Gamma_D = \Gamma$ and $u_D \equiv 0$ and the solution $(\sigma(\hat{\mathcal{T}}), u(\hat{\mathcal{T}})) \in \widetilde{\Sigma}(\hat{\mathcal{T}}) \times V(\hat{\mathcal{T}})$ to (3.3) with respect to $\hat{\mathcal{T}}$. Define the weighted norm $\|\bullet\|_A := (A\bullet, \bullet)^{1/2}$ in $L^2(\Omega; \mathbb{S})$.

Theorem 3.3 (reliability and efficiency). *There exist positive constants C_{Rel} and C_{Eff} depending on the shape regularity of $\hat{\mathcal{T}}$ such that*

$$(3.6) \quad \|\sigma - \sigma(\hat{\mathcal{T}})\|_A^2 \leq C_{Rel}(\eta^2(\hat{\mathcal{T}}) + \text{osc}^2(f, \hat{\mathcal{T}})) \quad (\text{reliability}),$$

$$(3.7) \quad \eta^2(\hat{\mathcal{T}}) \leq C_{Eff} \|\sigma - \sigma(\hat{\mathcal{T}})\|_A^2 \quad (\text{efficiency}).$$

Proof. The reliability and efficiency of the error estimator for the mixed finite element method [21, 24] in Subsect. 2.3 have been investigated in [18]. Note that the extended stress space $\widetilde{\Sigma}(\hat{\mathcal{T}})$ only differs from the stress space $\Sigma(\hat{\mathcal{T}})$ in (2.3) in the vertex degrees of freedom. Therefore, an analogy argument in [18, Thm. 3.1] can be applied to prove the reliability (3.6), and in [18, Thm. 3.2] can be applied to prove the efficiency (3.7). The details are omitted in this paper. Nevertheless, the discrete reliability in Theorem 3.9 below will lead to the reliability. \square

Let $\widetilde{\Sigma}(\mathcal{T}_\ell)$ denote the space in (3.2) and $V(\mathcal{T}_\ell)$ denote the space in (2.7) with respect to the triangulation \mathcal{T}_ℓ for $\ell \in \mathbb{N}_0$ from the following adaptive algorithm.

Algorithm: Adaptive algorithm for the nested mixed FEM

Given a parameter $0 < \theta < 1$ and an initial triangulation \mathcal{T}_0 . Set $\ell := 0$.

- **SOLVE:** Solve (3.3) with respect to \mathcal{T}_ℓ for the solution $(\sigma(\mathcal{T}_\ell), u(\mathcal{T}_\ell)) \in \widetilde{\Sigma}(\mathcal{T}_\ell) \times V(\mathcal{T}_\ell)$.
- **ESTIMATE:** Compute the error indicator $\eta^2(\mathcal{T}_\ell)$ of (3.5).
- **MARK:** Mark a set $\mathcal{M}_\ell \subset \mathcal{T}_\ell$ with (almost) minimal cardinality with

$$\theta(\eta^2(\mathcal{T}_\ell) + \text{osc}^2(f, \mathcal{T}_\ell)) \leq \eta^2(\mathcal{T}_\ell, \mathcal{M}_\ell) + \text{osc}^2(f, \mathcal{M}_\ell).$$

- **REFINE:** Refine each triangle K in \mathcal{M}_ℓ by NVB to get $\mathcal{T}_{\ell+1}$.
 - Set $\ell := \ell + 1$ and go to Step **SOLVE**.
-

3.3. Optimal convergence. Since the residual-based estimator is employed, the main task of optimality analysis is to prove the quasi-orthogonality and the discrete reliability.

Let $(\sigma(\mathcal{T}), u(\mathcal{T})) \in \widetilde{\Sigma}(\mathcal{T}) \times V(\mathcal{T})$ (resp. $(\sigma(\hat{\mathcal{T}}), u(\hat{\mathcal{T}})) \in \widetilde{\Sigma}(\hat{\mathcal{T}}) \times V(\hat{\mathcal{T}})$) solve (3.3) with respect to $\mathcal{T} \in \mathbb{T}$ (resp. its refinement $\hat{\mathcal{T}}$). Recall the L^2 projection $Q_{\mathcal{T}}$ (resp. $Q_{\hat{\mathcal{T}}}$) onto

$V(\mathcal{T})$ (resp. $V(\hat{\mathcal{T}})$). The analysis of the quasi-orthogonality and the discrete reliability requires the intermediate solution $(\hat{\sigma}(\hat{\mathcal{T}}), \hat{u}(\hat{\mathcal{T}})) \in \widetilde{\Sigma}(\hat{\mathcal{T}}) \times V(\hat{\mathcal{T}})$ with

$$(3.8) \quad \begin{cases} (A\hat{\sigma}(\hat{\mathcal{T}}), \tau(\hat{\mathcal{T}})) + (\operatorname{div}\tau(\hat{\mathcal{T}}), \hat{u}(\hat{\mathcal{T}})) = 0 & \text{for all } \tau(\hat{\mathcal{T}}) \in \widetilde{\Sigma}(\hat{\mathcal{T}}), \\ (\operatorname{div}\hat{\sigma}(\hat{\mathcal{T}}), v(\hat{\mathcal{T}})) = (Q_{\mathcal{T}}f, v(\hat{\mathcal{T}})) & \text{for all } v(\hat{\mathcal{T}}) \in V(\hat{\mathcal{T}}). \end{cases}$$

Lemma 3.4. *Let $(\sigma(\hat{\mathcal{T}}), u(\hat{\mathcal{T}})) \in (\widetilde{\Sigma}(\hat{\mathcal{T}}), V(\hat{\mathcal{T}}))$ solve (3.3), and let $(\hat{\sigma}(\hat{\mathcal{T}}), \hat{u}(\hat{\mathcal{T}})) \in (\widetilde{\Sigma}(\hat{\mathcal{T}}), V(\hat{\mathcal{T}}))$ solve (3.8). Then it holds*

$$\|\sigma(\hat{\mathcal{T}}) - \hat{\sigma}(\hat{\mathcal{T}})\|_A \lesssim \operatorname{osc}(f, \mathcal{T} \setminus \hat{\mathcal{T}}).$$

Proof. Given any $f \in L^2(\Omega; \mathbb{R}^2)$, write the mixed formulation for linear elasticity (2.1) with $\Gamma_D = \Gamma$ and $u_D \equiv 0$ as $\mathcal{L}(\sigma, u) = f$. Let $(\xi, z) = \mathcal{L}^{-1}((1 - Q_{\mathcal{T}})Q_{\hat{\mathcal{T}}}f)$. A stability result as in [18, Lemma 3.1] shows

$$(3.9) \quad \|\xi\|_A \lesssim \operatorname{osc}(Q_{\hat{\mathcal{T}}}f, \mathcal{T}) = \operatorname{osc}(Q_{\hat{\mathcal{T}}}f, \mathcal{T} \setminus \hat{\mathcal{T}}).$$

Note that $(\sigma(\hat{\mathcal{T}}) - \hat{\sigma}(\hat{\mathcal{T}}), u(\hat{\mathcal{T}}) - \hat{u}(\hat{\mathcal{T}}))$ is an approximation to (ξ, z) with respect to $\hat{\mathcal{T}}$. The best L^2 approximation [8] leads to

$$\|\xi - (\sigma(\hat{\mathcal{T}}) - \hat{\sigma}(\hat{\mathcal{T}}))\|_A \lesssim \inf_{\tau(\hat{\mathcal{T}}) \in \widetilde{\Sigma}(\hat{\mathcal{T}})} \|\xi - \tau(\hat{\mathcal{T}})\|_A \leq \|\xi\|_A.$$

This, (3.9) and a triangle inequality conclude the proof. \square

Theorem 3.5 (quasi-orthogonality). *For any $0 < \delta < 1$, there exists $C_0 > 0$ such that*

$$(1 - \delta)\|\sigma - \sigma(\hat{\mathcal{T}})\|_A^2 \leq \|\sigma - \sigma(\mathcal{T})\|_A^2 - \|\sigma(\hat{\mathcal{T}}) - \sigma(\mathcal{T})\|_A^2 + \frac{C_0}{\delta} \operatorname{osc}^2(f, \mathcal{T} \setminus \hat{\mathcal{T}}).$$

Proof. Recall $\hat{\sigma}(\hat{\mathcal{T}})$ from (3.8). Since $\operatorname{div}(\hat{\sigma}(\hat{\mathcal{T}}) - \sigma(\mathcal{T})) = 0$, the choice $\tau(\hat{\mathcal{T}}) = \hat{\sigma}(\hat{\mathcal{T}}) - \sigma(\mathcal{T})$ in (3.3) leads to

$$\begin{aligned} (A(\sigma - \sigma(\hat{\mathcal{T}})), \sigma(\hat{\mathcal{T}}) - \sigma(\mathcal{T})) &= (A(\sigma - \sigma(\hat{\mathcal{T}})), \sigma(\hat{\mathcal{T}}) - \hat{\sigma}(\hat{\mathcal{T}}) + \hat{\sigma}(\hat{\mathcal{T}}) - \sigma(\mathcal{T})) \\ &= (A(\sigma - \sigma(\hat{\mathcal{T}})), \sigma(\hat{\mathcal{T}}) - \hat{\sigma}(\hat{\mathcal{T}})). \end{aligned}$$

This and Lemma 3.4 show that there exists some constant $C_0 > 0$ such that

$$(A(\sigma - \sigma(\hat{\mathcal{T}})), \sigma(\hat{\mathcal{T}}) - \sigma(\mathcal{T})) \leq \sqrt{C_0} \|\sigma - \sigma(\hat{\mathcal{T}})\|_A \operatorname{osc}(f, \mathcal{T} \setminus \hat{\mathcal{T}}).$$

The combination with Young's inequality concludes the proof. \square

The analysis of the discrete reliability requires some $H^2(\Omega)$ conforming element. Recall the subdomains $\omega_{\mathbf{x}_e}^+$ and $\omega_{\mathbf{x}_e}^-$ in (2.2). The following H^2 conforming finite element space $S^{k+2}(\hat{\mathcal{T}})$ for $k \geq 3$ from [15] approximating $H^2(\Omega)$ extends the higher order Argyris finite element space by a modification around the vertices. The space reads

$$(3.10) \quad S^{k+2}(\hat{\mathcal{T}}) := \{\phi \in L^2(\Omega) \mid \forall K \in \hat{\mathcal{T}} \phi|_K \in P_{k+2}(K; \mathbb{R}); \phi \text{ and } \nabla\phi \text{ are continuous at all vertices, } \nabla\phi \text{ are continuous across all interior edges, } \nabla^2\phi \text{ are continuous at each initial vertex } \mathbf{x} \in \mathcal{V}(\mathcal{T}_0) \text{ and each boundary vertex } \mathbf{x} \in \mathcal{V}(\hat{\mathcal{T}}) \setminus \mathcal{V}_0(\hat{\mathcal{T}}), n_e^T \nabla^2 \phi t_e \text{ and } t_e^T \nabla^2 \phi t_e \text{ are continuous at each internal vertex } \mathbf{x}_e \in \mathcal{V}_0(\hat{\mathcal{T}}) \setminus \mathcal{V}(\mathcal{T}_0), n_e^T \nabla^2 \phi n_e \text{ is continuous at } \mathbf{x}_e \text{ in } \omega_{\mathbf{x}}^+ \text{ and at } \mathbf{x}_e \text{ in } \omega_{\mathbf{x}_e}^- \text{ for each } \mathbf{x}_e \in \mathcal{V}_0(\hat{\mathcal{T}}) \setminus \mathcal{V}(\mathcal{T}_0)\}.$$

Unlike functions in the higher order Argyris finite element space, the component $n_e^T \nabla^2 \phi(\hat{\mathcal{T}}) n_e$ of the second derivatives of function $\phi(\hat{\mathcal{T}}) \in S^{k+2}(\hat{\mathcal{T}})$ is not necessarily continuous at all internal vertices $\mathbf{x}_e \in \mathcal{V}_0(\hat{\mathcal{T}}) \setminus \mathcal{V}(\mathcal{T}_0)$.

Lemma 3.6 (discrete Helmholtz decomposition). *Given any $\tau(\hat{\mathcal{T}}) \in \widetilde{\Sigma}(\hat{\mathcal{T}})$ with $\operatorname{div} \tau(\hat{\mathcal{T}}) = 0$, there exists $\phi(\hat{\mathcal{T}}) \in S^{k+2}(\hat{\mathcal{T}})$ such that $\tau(\hat{\mathcal{T}}) = \operatorname{CurlCurl} \phi(\hat{\mathcal{T}})$.*

Proof. The proof is given by counting the dimensions. Let

$$K_{\hat{\mathcal{T}}}(\operatorname{div}) := \{\tau(\hat{\mathcal{T}}) \in \widetilde{\Sigma}(\hat{\mathcal{T}}) \mid \operatorname{div} \tau(\hat{\mathcal{T}}) = 0\}$$

denote the discrete divergence kernel space with respect to $\widetilde{\Sigma}(\hat{\mathcal{T}})$. Note that $\operatorname{CurlCurl} S^{k+2}(\hat{\mathcal{T}})$ is a subspace of $K_{\hat{\mathcal{T}}}(\operatorname{div})$, namely, $\operatorname{CurlCurl} S^{k+2}(\hat{\mathcal{T}}) \subseteq K_{\hat{\mathcal{T}}}(\operatorname{div})$. The dimension of $K_{\hat{\mathcal{T}}}(\operatorname{div})$ is equal to the difference between the dimension of $\widetilde{\Sigma}(\hat{\mathcal{T}})$ and the dimension of $V(\hat{\mathcal{T}})$, this is

$$\begin{aligned} & 3|\mathcal{V}(\hat{\mathcal{T}})| + |\mathcal{V}_0(\hat{\mathcal{T}}) \setminus \mathcal{V}(\mathcal{T}_0)| + 2(k-1)|\hat{\mathcal{E}}| + \frac{3k(k-1)}{2}|\hat{\mathcal{T}}| - k(k+1)|\hat{\mathcal{T}}| \\ &= 3|\mathcal{V}(\hat{\mathcal{T}})| + |\mathcal{V}_0(\hat{\mathcal{T}}) \setminus \mathcal{V}(\mathcal{T}_0)| + 2(k-1)|\hat{\mathcal{E}}| + \frac{k(k-5)}{2}|\hat{\mathcal{T}}|. \end{aligned}$$

The dimension of $\operatorname{CurlCurl} S^{k+2}(\hat{\mathcal{T}})$ is

$$6|\mathcal{V}(\hat{\mathcal{T}})| + |\mathcal{V}_0(\hat{\mathcal{T}}) \setminus \mathcal{V}(\mathcal{T}_0)| + (2k-5)|\hat{\mathcal{E}}| + \frac{(k-2)(k-3)}{2}|\hat{\mathcal{T}}| - 3.$$

Since Ω is simply-connected, Euler's formula holds that

$$|\mathcal{V}(\hat{\mathcal{T}})| - |\hat{\mathcal{E}}| + |\hat{\mathcal{T}}| = 1.$$

This shows that

$$\dim \operatorname{CurlCurl} S^{k+2}(\hat{\mathcal{T}}) = \dim K_{\hat{\mathcal{T}}}(\operatorname{div})$$

and consequently implies that

$$\operatorname{CurlCurl} S^{k+2}(\hat{\mathcal{T}}) = K_{\hat{\mathcal{T}}}(\operatorname{div}).$$

This concludes the proof. \square

Lemma 3.7 (quasi-interpolation). *Suppose $S^{k+2}(\mathcal{T})$ (resp. $S^{k+2}(\hat{\mathcal{T}})$) denotes the space in (3.10) with respect to \mathcal{T} (resp. its refinement $\hat{\mathcal{T}}$). There exists a quasi-interpolation $\Pi_{\mathcal{T}, \nabla^2} : S^{k+2}(\hat{\mathcal{T}}) \rightarrow S^{k+2}(\mathcal{T})$, which preserves the value of the function at all vertices of \mathcal{T} , for any $\phi(\hat{\mathcal{T}}) \in S^{k+2}(\hat{\mathcal{T}})$,*

- (a) for any $\mathbf{x} \in \mathcal{V}(\mathcal{T})$, $\Pi_{\mathcal{T}, \nabla^2} \phi(\hat{\mathcal{T}})(\mathbf{x}) = \phi(\hat{\mathcal{T}})(\mathbf{x})$;
- (b) for any $K \in \mathcal{T} \setminus \hat{\mathcal{T}}$, $\Pi_{\mathcal{T}, \nabla^2} \phi(\hat{\mathcal{T}})|_K = \phi(\hat{\mathcal{T}})|_K$;
- (c) for any $K \in \mathcal{T}$ with patch $\Omega(K) := \operatorname{int}(\cup \{K' \in \mathcal{T} \mid \operatorname{dist}(K, K') = 0\})$,

$$(3.11) \quad \sum_{m=0}^2 h_K^{m-2} |\phi(\hat{\mathcal{T}}) - \Pi_{\mathcal{T}, \nabla^2} \phi(\hat{\mathcal{T}})|_{m,K} \leq C_{\text{apx}} |\phi(\hat{\mathcal{T}})|_{2, \Omega(K)}$$

with a constant C_{apx} that only depends on the shape regularity of \mathcal{T}_0 .

Proof. The quasi-interpolation for $S^{k+2}(\hat{\mathcal{T}})$ was constructed in [15] by adopting the quasi-interpolation for the higher order Argyris finite element space in [19] to the extended Argyris element considered therein. It was proven in [15] that that quasi-interpolation satisfies (b)-(c). In order to preserve the value of the function at all vertices of \mathcal{T} , it can be done by replacing the combination coefficient of the basis functions associated with the vertex

function value degrees of freedom by the value of functions at these vertices, namely, it is imposed as

$$\Pi_{\mathcal{T}, \nabla^2} \phi(\hat{\mathcal{T}})(x) = \phi(\hat{\mathcal{T}})(x) \text{ for any } x \in \mathcal{V}(\mathcal{T}).$$

This concludes the proof. \square

Lemma 3.8. *Let $(\sigma(\mathcal{T}), u(\mathcal{T})) \in (\widetilde{\Sigma}(\mathcal{T}), V(\mathcal{T}))$ solve (3.3) with respect to \mathcal{T} , and let $(\hat{\sigma}(\hat{\mathcal{T}}), \hat{u}(\hat{\mathcal{T}})) \in (\widetilde{\Sigma}(\hat{\mathcal{T}}), V(\hat{\mathcal{T}}))$ solve (3.8). Then it holds*

$$\|\sigma(\mathcal{T}) - \hat{\sigma}(\hat{\mathcal{T}})\|_A^2 \lesssim \eta^2(\mathcal{T}, \mathcal{T} \setminus \hat{\mathcal{T}}).$$

Proof. Let $\xi(\hat{\mathcal{T}}) := \sigma(\mathcal{T}) - \hat{\sigma}(\hat{\mathcal{T}})$. Since $\operatorname{div} \xi(\hat{\mathcal{T}}) = 0$, Lemma 3.6 implies that there exists $\phi(\hat{\mathcal{T}}) \in S^{k+2}(\hat{\mathcal{T}})$ such that $\xi(\hat{\mathcal{T}}) = \operatorname{Curl} \operatorname{Curl} \phi(\hat{\mathcal{T}})$. Recall the quasi-interpolation $\Pi_{\mathcal{T}, \nabla^2}$ from Lemma 3.7 and let $\psi(\hat{\mathcal{T}}) := \phi(\hat{\mathcal{T}}) - \Pi_{\mathcal{T}, \nabla^2} \phi(\hat{\mathcal{T}}) \in S^{k+2}(\hat{\mathcal{T}})$. The choice $\tau(\hat{\mathcal{T}}) = \xi(\hat{\mathcal{T}})$ in (3.8) and the choice $\tau(\mathcal{T}) = \operatorname{Curl} \operatorname{Curl}(\Pi_{\mathcal{T}, \nabla^2} \phi(\hat{\mathcal{T}}))$ in (3.3) with respect to \mathcal{T} plus (b) of Lemma 3.7 show

$$\begin{aligned} \|\xi(\hat{\mathcal{T}})\|_A^2 &= (A(\sigma(\mathcal{T}) - \hat{\sigma}(\hat{\mathcal{T}})), \xi(\hat{\mathcal{T}})) = (A\sigma(\mathcal{T}), \operatorname{Curl} \operatorname{Curl} \psi(\hat{\mathcal{T}})) \\ &= \sum_{K \in \mathcal{T} \setminus \hat{\mathcal{T}}} (A\sigma(\mathcal{T}), \operatorname{Curl} \operatorname{Curl} \psi(\hat{\mathcal{T}}))_K. \end{aligned}$$

An integration by parts leads to

$$\begin{aligned} \|\xi(\hat{\mathcal{T}})\|_A^2 &= \sum_{K \in \mathcal{T} \setminus \hat{\mathcal{T}}} \left((\operatorname{curl} \operatorname{curl}(A\sigma(\mathcal{T})), \psi(\hat{\mathcal{T}}))_K + \sum_{e \in \mathcal{E}(K)} (\langle A\sigma(\mathcal{T})t \cdot t, \operatorname{Curl} \psi(\hat{\mathcal{T}}) \cdot t \rangle_e \right. \\ (3.12) \quad &\quad \left. - \langle \operatorname{curl}(A\sigma(\mathcal{T})) \cdot t, \psi(\hat{\mathcal{T}}) \rangle_e) + \sum_{e \in \mathcal{E}(K)} \langle A\sigma(\mathcal{T})t \cdot n, \operatorname{Curl} \psi(\hat{\mathcal{T}}) \cdot n \rangle_e \right). \end{aligned}$$

Since the compliance tensor A is symmetric and continuous, $(A\sigma(\mathcal{T})t) \cdot n = (A\sigma(\mathcal{T})n) \cdot t = (t^T \sigma(\mathcal{T})n)/(2\mu)$ is continuous across interior edge e . Since (a) of Lemma 3.7 guarantees that $\psi(\hat{\mathcal{T}})$ vanishes at each vertex $x \in \mathcal{V}(\mathcal{T})$, an integration by parts results in

$$\begin{aligned} \sum_{K \in \mathcal{T} \setminus \hat{\mathcal{T}}} \sum_{e \in \mathcal{E}(K)} \langle A\sigma(\mathcal{T})t \cdot n, \operatorname{Curl} \psi(\hat{\mathcal{T}}) \cdot n \rangle_e &= - \sum_{K \in \mathcal{T} \setminus \hat{\mathcal{T}}} \sum_{e \in \mathcal{E}(\Gamma) \cap \mathcal{E}(K)} \langle A\sigma(\mathcal{T})t_e \cdot n_e, \partial_{t_e} \psi(\hat{\mathcal{T}}) \rangle_e \\ &= \sum_{K \in \mathcal{T} \setminus \hat{\mathcal{T}}} \sum_{e \in \mathcal{E}(\Gamma) \cap \mathcal{E}(K)} \langle \partial_{t_e} (A\sigma(\mathcal{T})t_e \cdot n_e), \psi(\hat{\mathcal{T}}) \rangle_e, \end{aligned}$$

This and (3.12) lead to

$$\|\xi(\hat{\mathcal{T}})\|_A^2 \leq \sum_{K \in \mathcal{T} \setminus \hat{\mathcal{T}}} \eta^2(\mathcal{T}, K) \left(h_K^{-4} \|\psi(\hat{\mathcal{T}})\|_{0,K}^2 + \sum_{e \in \mathcal{E}(K)} (h_K^{-1} \|\operatorname{Curl} \psi(\hat{\mathcal{T}})\|_{0,e}^2 + 2h_K^{-3} \|\psi(\hat{\mathcal{T}})\|_{0,e}^2) \right)^{1/2}.$$

Trace inequalities, the estimates in (3.11) for $\psi(\hat{\mathcal{T}}) = \phi(\hat{\mathcal{T}}) - \Pi_{\mathcal{T}, \nabla^2} \phi(\hat{\mathcal{T}})$ and $|\phi(\hat{\mathcal{T}})|_2 \lesssim \|\xi(\hat{\mathcal{T}})\|_0$ prove

$$(3.13) \quad \|\xi(\hat{\mathcal{T}})\|_A^2 \lesssim \sum_{K \in \mathcal{T} \setminus \hat{\mathcal{T}}} \eta(\mathcal{T}, K) |\phi(\hat{\mathcal{T}})|_{2, \Omega(K)} \lesssim \eta(\mathcal{T}, \mathcal{T} \setminus \hat{\mathcal{T}}) \|\xi(\hat{\mathcal{T}})\|_0.$$

Since $\operatorname{div} \xi(\hat{\mathcal{T}}) = 0$ and $\int_{\Omega} \operatorname{tr} \xi(\hat{\mathcal{T}}) dx = \int_{\Omega} \operatorname{tr}(\sigma(\mathcal{T}) - \hat{\sigma}(\hat{\mathcal{T}})) dx = 0$, Proposition 9.1.1 of [9] shows

$$\|\xi(\hat{\mathcal{T}})\|_0 \lesssim \|\xi(\hat{\mathcal{T}})\|_A.$$

The combination with (3.13) concludes the proof. \square

Theorem 3.9 (discrete reliability). *There exists a positive constant C such that*

$$\|\sigma(\hat{\mathcal{T}}) - \sigma(\mathcal{T})\|_A^2 \leq C(\eta^2(\mathcal{T}, \mathcal{T} \setminus \hat{\mathcal{T}}) + \text{osc}^2(f, \mathcal{T} \setminus \hat{\mathcal{T}})).$$

Proof. A triangle inequality plus Lemma 3.4 and 3.8 conclude the proof. \square

With the quasi-orthogonality in Theorem 3.5 and the discrete reliability in Theorem 3.9, the analysis as in [10, 16, 23, 27, 28] will lead to the convergence and optimal convergence of the adaptive algorithm in Subsect. 3.2.

Lemma 3.10 (estimator reduction). *Let $(\sigma(\mathcal{T}_\ell), u(\mathcal{T}_\ell)) \in \widetilde{\Sigma}(\mathcal{T}_\ell) \times V(\mathcal{T}_\ell)$ solve (3.3) over the nested triangulations \mathcal{T}_ℓ and $\mathcal{T}_{\ell-1}$, respectively. Then given any positive constant ϵ , there exists $\lambda := 1 - 2^{-1/2} < 1$ and $C_\epsilon > 0$ such that*

$$\eta^2(\mathcal{T}_\ell) \leq (1 + \epsilon)(\eta^2(\mathcal{T}_{\ell-1}) - \lambda\eta^2(\mathcal{T}_{\ell-1}, \mathcal{M}_{\ell-1})) + C_\epsilon\|\sigma(\mathcal{T}_\ell) - \sigma(\mathcal{T}_{\ell-1})\|_A^2$$

and

$$\text{osc}^2(f, \mathcal{T}_\ell) \leq \text{osc}^2(f, \mathcal{T}_{\ell-1}) - \lambda \text{osc}^2(f, \mathcal{T}_\ell \setminus \mathcal{T}_{\ell+1}).$$

Proof. The proof follows the same arguments as in [16, Corollary 4.4]. \square

Theorem 3.11. *Given $f \in L^2(\Omega; \mathbb{R}^2)$, let (σ, u) denote the exact solution of (2.1), and $(\sigma(\mathcal{T}_\ell), u(\mathcal{T}_\ell))$ and $(\sigma(\mathcal{T}_{\ell-1}), u(\mathcal{T}_{\ell-1}))$ denote the discrete solutions over the nested triangulations \mathcal{T}_ℓ and $\mathcal{T}_{\ell-1}$, respectively. Then there exist positive constants $0 < \alpha < 1$, $\beta > 0$, $\gamma > 0$ such that*

$$E_\ell \leq \alpha E_{\ell-1}$$

with

$$E_\ell = \|\sigma - \sigma(\mathcal{T}_\ell)\|_A^2 + \gamma\eta^2(\mathcal{T}_\ell) + (\beta + \gamma)\text{osc}^2(f, \mathcal{T}_\ell).$$

Proof. Lemma 3.10, the reliability (3.6) and the quasi-orthogonality conclude the proof. See the details in [10, 23, 28]. \square

For $s > 0$, define the approximation class \mathbb{A}_s as

$$\mathbb{A}_s = \left\{ (\sigma, f) : |\sigma, f|_s < \infty \text{ with } |\sigma, f|_s := \sup_{N>0} (N^s \inf_{|\mathcal{T}|=N} \inf_{\tau \in \widetilde{\Sigma}(\mathcal{T})} \|\sigma - \tau\|_A^2 + \text{osc}^2(f, \mathcal{T})) \right\}.$$

Theorem 3.12 (optimality). *Let \mathcal{M}_ℓ be a set of marked elements with minimal cardinality, (σ, u) the solution of (2.1), and $(\mathcal{T}_\ell, \widetilde{\Sigma}(\mathcal{T}_\ell) \times V(\mathcal{T}_\ell), \sigma(\mathcal{T}_\ell), u(\mathcal{T}_\ell))$ the sequence of triangulations, finite element spaces, and discrete solutions produced by the adaptive FEMs with the marking parameter θ . Then it holds that*

$$\|\sigma - \sigma(\mathcal{T}_\ell)\|_A^2 + \text{osc}^2(f, \mathcal{T}_\ell) \lesssim |\sigma, f|_s (|\mathcal{T}_\ell| - |\mathcal{T}_0|)^{-s} \text{ for } (\sigma, f) \in \mathbb{A}_s.$$

Proof. This follows from [10, 23, 28] with Lemma 3.10, the quasi-orthogonality, the discrete reliability and the efficiency (3.7). \square

4. EXTENDED STRESS SPACES AT VERTEX CORNERS

This section is devoted to treat the boundary condition with $|\Gamma_N| > 0$ and $g \neq 0$ in (2.1).

4.1. Two dimensional case. Recall the discrete stress space $\Sigma(\hat{\mathcal{T}})$ in (2.3). To impose the general traction boundary condition g on Γ_N , it requires some approximation $g(\hat{\mathcal{T}}) = \alpha(\hat{\mathcal{T}})n|_{\Gamma_N}$ with $\alpha(\hat{\mathcal{T}}) \in \Sigma(\hat{\mathcal{T}})$. Since $\alpha(\hat{\mathcal{T}})$ is continuous at each boundary vertex, $g(\hat{\mathcal{T}})$ may not be taken as the nodal interpolation of g . To see it, consider a situation depicted in Figure 4.1(a) where a corner vertex \mathbf{x}_c on the boundary of the polygonal domain Ω is the unique intersected point of two boundary edges e_+ and e_- . Let t_i and n_i denote the unit tangential and outward normal vectors of e_i , $i = +, -$. If the traction boundary condition $g|_{e_i}$, $i = +, -$ is consistent (continuous) in the sense that $(n_-^T g|_{e_+})(\mathbf{x}_c) = (n_+^T g|_{e_-})(\mathbf{x}_c)$, the usual nodal interpolation can be well defined as follows

$$(4.1) \quad S_{11}\varphi_{\mathbf{x}_c}(\mathbf{x})\mathbb{S}_1 + S_{12}\varphi_{\mathbf{x}_c}(\mathbf{x})\mathbb{S}_2 + S_{22}\varphi_{\mathbf{x}_c}(\mathbf{x})\mathbb{S}_3 + \tau$$

with $\tau \in \Sigma(\hat{\mathcal{T}})$ and vanishes at \mathbf{x}_c . Recall that $\varphi_{\mathbf{x}_c}(\mathbf{x})$ is the nodal basis function associated to vertex \mathbf{x}_c of the scalar-valued Lagrange element of order k , and \mathbb{S}_i is a canonical basis of the symmetric matrix space \mathbb{S} . The combination coefficients S_{11} , S_{12} , S_{22} are three components of the solution $S \in \mathbb{S}$ of the following system of equations:

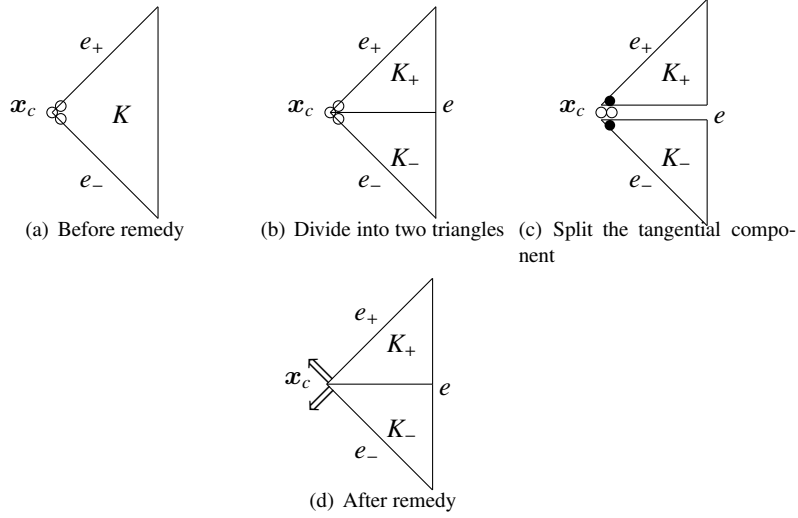
$$\begin{cases} n_+^T S n_+ = (n_+^T g|_{e_+})(\mathbf{x}_c), \\ n_-^T S n_- = (n_-^T g|_{e_-})(\mathbf{x}_c), \\ n_+^T S n_- = (n_+^T g|_{e_-})(\mathbf{x}_c). \end{cases}$$

However, a general traction boundary condition can be inconsistent (discontinuous) in the sense that $n_-^T g|_{e_+}(\mathbf{x}_c) \neq n_+^T g|_{e_-}(\mathbf{x}_c)$. Such inconsistency (discontinuity) causes an essential difficulty for imposing such a boundary condition for the discrete stress space $\Sigma(\hat{\mathcal{T}})$. In particular, the usual nodal interpolation as in (4.1) might not be defined since the combination coefficients S_{11} , S_{12} , and S_{22} have to satisfy the following four equations

$$\begin{cases} n_+^T S n_+ = (n_+^T g|_{e_+})(\mathbf{x}_c), \\ n_-^T S n_- = (n_-^T g|_{e_-})(\mathbf{x}_c), \\ n_+^T S n_- = (n_+^T g|_{e_-})(\mathbf{x}_c), \\ n_-^T S n_+ = (n_-^T g|_{e_+})(\mathbf{x}_c), \end{cases}$$

while because of the inconsistency, there does not exist a solution of the above system of equations. As a result, the traction boundary condition can not be exactly imposed even if $g|_{e_i}$, $i = +, -$, is a polynomial of degree not bigger than k for this case. The least-square constraint was employed in [13] to deal with this case. The subsequent analysis extends the treatment of non-nestedness in Subsect. 3.1 to allow for an exact nodal interpolation at corner vertices.

The idea to overcome such a difficulty is to split the triangle at the corner into two sub-triangles and then relax the continuity of the pure tangential component across the common edge of these two sub-triangles. In order to accomplish this, first divide K into a patch consisting of two triangles K_+ and K_- and $e = K_+ \cap K_-$ in Figure 4.1(b). The pure tangential component of discrete stress does not have to be continuous across e at \mathbf{x}_c . Therefore, one can split this degree of freedom into two separate degrees of freedom in K_+ and K_- , respectively. In Figure 4.1(c), the solid points represent these two separate degrees of freedom and the two circles represent the degrees of freedom of normal components across e . In order to define the nodal interpolation, the four basis functions associated to vertex \mathbf{x}_c , as depicted in Figure 4.1(d), of the extended stress space will be presented as

FIGURE 4.1. Degrees of freedom at corner vertex x_c

follows

$$(4.2) \quad \begin{aligned} \tau_1 = \varphi_{x_c} \begin{cases} \mathbb{S}_{e_+,1}^\perp + c_1 \mathbb{S}_{e_+} & \text{on } K_+ \\ d_1 \mathbb{S}_{e_-} & \text{on } K_- \end{cases}, \quad \tau_2 = \varphi_{x_c} \begin{cases} \mathbb{S}_{e_+,2}^\perp + c_2 \mathbb{S}_{e_+} & \text{on } K_+ \\ d_2 \mathbb{S}_{e_-} & \text{on } K_- \end{cases} \\ \tau_3 = \varphi_{x_c} \begin{cases} c_3 \mathbb{S}_{e_+} & \text{on } K_+ \\ \mathbb{S}_{e_-,1}^\perp + d_3 \mathbb{S}_{e_-} & \text{on } K_- \end{cases}, \quad \tau_4 = \varphi_{x_c} \begin{cases} c_4 \mathbb{S}_{e_+} & \text{on } K_+ \\ \mathbb{S}_{e_-,2}^\perp + d_4 \mathbb{S}_{e_-} & \text{on } K_- \end{cases} \end{aligned}$$

with the Lagrange nodal basis function φ_{x_c} associated to x_c and the other notation defined in Section 2. One can compute the constants c_i, d_i for $1 \leq i \leq 4$ by using the normal continuity of τ_i across e . For instance, given the normal vector n_e of e , the normal continuity of τ_1 results in the following equations

$$(4.3) \quad (\mathbb{S}_{e_+,1}^\perp + c_1 \mathbb{S}_{e_+}) n_e = d_1 \mathbb{S}_{e_-} n_e.$$

Recall the definition of the matrix $\mathbb{S}_{e_+} = t_{e_+} t_{e_+}^T$ for edge e_+ with tangential vector t_{e_+} and the analogy for \mathbb{S}_{e_-} . Assuming $t_{e_+} = (a \ b)^T$, define its perpendicular row vector by $t_{e_+}^\perp = (b \ -a)$; $t_{e_-}^\perp$ is similar defined for t_{e_-} . Let D denote the determinant of the matrix $(t_{e_+} \ t_{e_-})$. Elementary computations eventually lead to the inverse matrix

$$(\mathbb{S}_{e_+} n_e - \mathbb{S}_{e_-} n_e)^{-1} = ((t_{e_+}^T n_e) t_{e_+} - (t_{e_-}^T n_e) t_{e_-})^{-1} = \frac{1}{D} \begin{pmatrix} \frac{1}{t_{e_+}^T n_e} t_{e_-}^\perp \\ \frac{1}{t_{e_-}^T n_e} t_{e_+}^\perp \end{pmatrix}.$$

There always exist unique c_1, d_1 to (4.3) unless e_+ is parallel to e_- .

Remark 4.1 (more triangles). *Suppose there are three triangles K_+, K, K_- with $e_1 = K_+ \cap K$ and $e_2 = K_- \cap K$ around the corner vertex x_c shown in Figure 4.2. In order to relax the C^0 continuity at x_c , a similar argument as in the case of two triangles leads to five new*

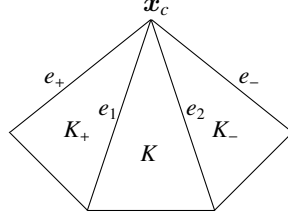


FIGURE 4.2. Three triangles

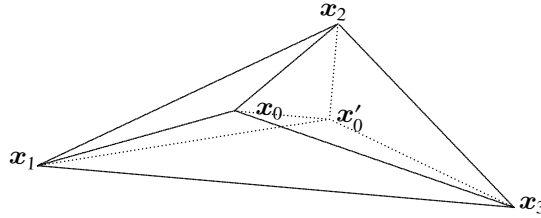
basis functions at x_c as follows:

$$(4.4) \quad \begin{aligned} \tau_1 = \varphi_{x_c} & \begin{cases} \mathbb{S}_{e_+,1}^\perp + c_1 \mathbb{S}_{e_+} & \text{on } K_+ \\ d_1 \mathbb{S}_{e_2} & \text{on } K \\ 0 & \text{on } K_- \end{cases}, \quad \tau_2 = \varphi_{x_c} \begin{cases} \mathbb{S}_{e_+,2}^\perp + c_2 \mathbb{S}_{e_+} & \text{on } K_+ \\ d_2 \mathbb{S}_{e_2} & \text{on } K \\ 0 & \text{on } K_- \end{cases}, \\ \tau_3 = \varphi_{x_c} & \begin{cases} 0 & \text{on } K_+ \\ c_3 \mathbb{S}_{e_1} & \text{on } K \\ \mathbb{S}_{e_-,1}^\perp + d_3 \mathbb{S}_{e_-} & \text{on } K_- \end{cases}, \quad \tau_4 = \varphi_{x_c} \begin{cases} 0 & \text{on } K_+ \\ c_4 \mathbb{S}_{e_1} & \text{on } K \\ \mathbb{S}_{e_-,2}^\perp + d_4 \mathbb{S}_{e_-} & \text{on } K_- \end{cases}, \\ \tau_5 = \varphi_{x_c} & \begin{cases} \mathbb{S}_{e_+} & \text{on } K_+ \\ c_5 \mathbb{S}_{e_1,1}^\perp + d_5 \mathbb{S}_{e_1,2}^\perp + g_5 \mathbb{S}_{e_1} & \text{on } K \\ h_5 \mathbb{S}_{e_-} & \text{on } K_- \end{cases}. \end{aligned}$$

Using the normal continuity of τ_j across e_1 can compute c_j, d_j for $j = 1, 2$. Using the normal continuity of τ_j across e_2 can compute c_j, d_j for $j = 3, 4$. Using the normal continuity across e_1 and e_2 of τ_5 can compute c_5, d_5, g_5, h_5 .

4.2. Comments for three dimensions. This subsection extends the discrete stress space of the mixed finite element on tetrahedral grids [21, 25] and only provides an outline. Apart from the C^0 continuity at vertices, the discrete stresses have some continuity across edges.

If there are inconsistency boundary conditions imposed on the intersection of three planes on Γ_N , it requires to deal with the degrees of freedom associated with vertices and edges. Given a tetrahedron $K := x_0 x_1 x_2 x_3$ in Figure 4.3, suppose x_0 denotes the corner vertex. In order to relax some continuity at vertices and edges, divide K into four sub-tetrahedra with the barycentre x'_0 . The goal is to compute the new basis functions associated with vertex x_0 and edges $x_0 x_1, x_0 x_2, x_0 x_3$ as those in (4.2). Let n_1, n_2 and n_3 denote the outnormal of face $F_1 := x_0 x_2 x_1$, face $F_2 := x_0 x_1 x_3$ and face $F_3 := x_0 x_3 x_2$ respectively.

FIGURE 4.3. Tetrahedron K

Given $1 \leq m \leq 3$, note that there exist three independent symmetric matrices $\mathbb{S}_{j,m}$ in each sub-tetrahedron $K_m = \text{conv}(\mathbf{x}'_0 \cup F_m)$ such that $\mathbb{S}_{j,m} \mathbf{n}_m = 0$, $1 \leq j \leq 3$ and three symmetric independent matrices $\mathbb{S}_{i,m}^\perp$ such that $\mathbb{S}_{i,m}^\perp : \mathbb{S}_{j,m} = 0$, $1 \leq i \leq 3$. Assume the following expression

$$\tau_{i,1} = \varphi_{\mathbf{x}_0} \begin{cases} \mathbb{S}_{i,1}^\perp + \sum_{j=1}^3 c_{j,1} \mathbb{S}_{j,1} & \text{on } K_1 \\ \sum_{j=1}^3 d_{j,1} \mathbb{S}_{j,2} & \text{on } K_2 \\ \sum_{j=1}^3 e_{j,1} \mathbb{S}_{j,3} & \text{on } K_3 \end{cases}$$

with the Lagrange basis function $\varphi_{\mathbf{x}_0}$ associated with \mathbf{x}_0 and nine constants $c_{j,1}, d_{j,1}, e_{j,1}$. It can be easily checked that $\tau_{i,1} \mathbf{n}_m|_{F_m} = 0$ for $m = 2, 3$. Using the normal continuity across the interior faces leads to the unique solutions $c_{j,1}, d_{j,1}, e_{j,1}$ as long as any two of F_m , $1 \leq m \leq 3$ do not lie in one plane. Hence $\tau_{i,1}$, $1 \leq i \leq 3$ are three new basis function associated with \mathbf{x}_0 . Similar arguments compute the other six functions associated with the vertex \mathbf{x}_0 .

As for any internal node \mathbf{a} in the edge $\mathbf{x}_0 \mathbf{x}_1$, define

$$\xi_{i,1} = \varphi_{\mathbf{a}} \begin{cases} \mathbb{S}_{i,1}^\perp + \sum_{j=1}^3 c_{j,1} \mathbb{S}_{j,1} & \text{on } K_1 \\ \sum_{j=1}^3 d_{j,1} \mathbb{S}_{j,2} & \text{on } K_2 \end{cases}$$

with the Lagrange basis function $\varphi_{\mathbf{a}}$ associated with \mathbf{a} and six constants $c_{j,1}, d_{j,1}$. It should be mentioned that the normal continuity across the interior face $\mathbf{x}_1 \mathbf{x}'_0 \mathbf{x}_0$ only imposes three conditions. Therefore, there exist some $H(\text{div})$ bubble functions on $K_1 \cup K_2$. Let t, t_1 and t_2 denote the tangential vector of edge $\mathbf{x}_0 \mathbf{x}_1, \mathbf{x}_0 \mathbf{x}_2, \mathbf{x}_0 \mathbf{x}_3$, and let n denote the normal vector of face $\mathbf{x}_1 \mathbf{x}'_0 \mathbf{x}_0$. The three $H(\text{div})$ bubble functions read

$$b_1 = \begin{cases} \varphi_{\mathbf{a}} t t^T & \text{on } K_1 \\ 0 & \text{on } K_2 \end{cases}, \quad b_2 = \begin{cases} 0 & \text{on } K_1 \\ \varphi_{\mathbf{a}} t t^T & \text{on } K_2 \end{cases}, \quad b_3 = \begin{cases} \frac{\varphi_{\mathbf{a}}}{t_1^T n} (t_1 t^T + t_1^T t) & \text{on } K_1 \\ \frac{\varphi_{\mathbf{a}}}{t_2^T n} (t_2 t^T + t_2^T t) & \text{on } K_2 \end{cases}.$$

Actually, b_1 (resp. b_2) is already the original $H(\text{div})$ bubble function on K_1 (resp. K_2) from [21, 25]. Unless F_1 and F_2 are parallel, there always exist the unique six constants $c_{j,1}, d_{j,1}$ with the constraint of the bubble functions. Hence $\xi_{i,1}$ for $1 \leq i \leq 3$ are three new basis function associated with edge $\mathbf{x}_0 \mathbf{x}_1$.

5. NUMERICS

This section provides five examples to compare the conforming mixed element of $k = 3$ in [24] introduced in Subsect. 2.3 before and after relaxing the C^0 vertex continuity of stress spaces. Example 5.2-5.4 show the results by relaxing the C^0 continuity at corner vertices in Subsect. 4.1 on uniform and adaptive meshes. The last example demonstrates convergence rates of the adaptive mixed finite element with nested stress spaces in Subsect. 3.1.

5.1. Interface problem. Let $\mathbf{x} = (x_1, x_2)^T$. Consider a piecewise constant stress $\sigma = \begin{pmatrix} \sigma_{11} & 0 \\ 0 & 0 \end{pmatrix}$ with a discontinuous pure tangential component σ_{11} across $x_2 = 0.5$ depicted in Figure 5.1(a). Suppose that the intersection of any edge of $\hat{\mathcal{T}}$ with $x_2 = 0.5$ is an empty set, a vertex or the edge itself. Recall the stress space $\Sigma(\hat{\mathcal{T}})$ in (2.3). Since any matrix-valued function in $\Sigma(\hat{\mathcal{T}})$ is C^0 continuous at each vertex of $\hat{\mathcal{T}}$. The mixed FEM (2.8) cannot achieve the exact stress due to $\sigma \notin \Sigma(\hat{\mathcal{T}})$.

For vertex \mathbf{a} on $x_2 = 0.5$ shown in Figure 5.1, employ the treatment in Subsect. 3.1 to split the degree of freedom with respect to the pure tangential component along $x_2 = 0.5$ into two degrees of freedom shared by the upper plane and lower plane, respectively. The

two solid points in Figure 5.1 represent the two new separate degrees of freedom; the two circles represent the degrees of freedom with respect to normal components. Deal with all vertices on $x_2 = 0.5$ analogously. An extended stress space $\widetilde{\Sigma}(\widetilde{\mathcal{T}})$ is then constructed by enriching $\Sigma(\widetilde{\mathcal{T}})$ with all the new functions whose pure tangential component are discontinuous across $x_2 = 0.5$.

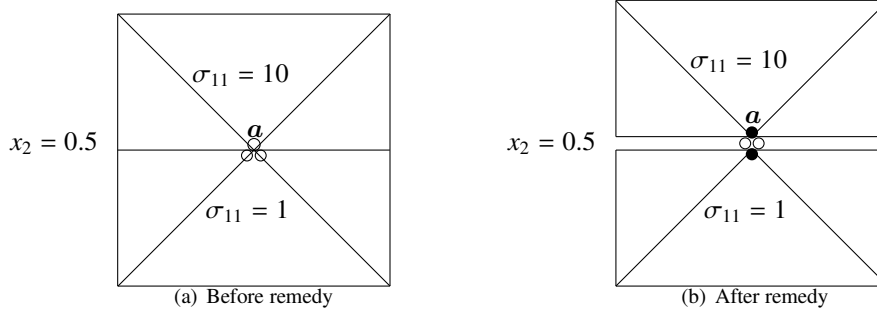


FIGURE 5.1. Degrees of freedom at vertex a

Consider the interpolation of σ in $\widetilde{\Sigma}(\widetilde{\mathcal{T}})$. Let the interpolation $I_{\widetilde{\mathcal{T}}}\sigma_{11}$ equal to 1 at vertex a in each element below $x_2 = 0.5$, and 10 in each element above. Thus $I_{\widetilde{\mathcal{T}}}\sigma_{11} = \sigma_{11}$. Since the computing error is less than the interpolation error, the mixed FEM with the extended stress space $\widetilde{\Sigma}(\widetilde{\mathcal{T}})$ computes the exact stress.

5.2. A benchmark problem over an L-shaped domain with treatment of corners on uniform meshes. Consider the model problem on the rotated L-shaped domain $\Omega \subset \mathbb{R}^2$ as depicted in Figure 5.2. The exact solution reads in polar coordinates

$$u_r(r, \phi) = \frac{r^\alpha}{2\mu} (-(\alpha + 1) \cos((\alpha + 1)\phi) + (C_2 - \alpha - 1)C_1 \cos((\alpha - 1)\phi)),$$

$$u_\phi(r, \phi) = \frac{r^\alpha}{2\mu} ((\alpha + 1) \sin((\alpha + 1)\phi) + (C_2 + \alpha - 1)C_1 \sin((\alpha - 1)\phi)).$$

The constants are $C_1 := -\cos((\alpha + 1)\omega) / \cos((\alpha - 1)\omega)$ and $C_2 := 2(\lambda + 2\mu) / (\lambda + \mu)$, where $\alpha = 0.544483736782$ is the positive solution of $\alpha \sin(2\omega) + \sin(2\omega\alpha) = 0$ for $\omega = 3\pi/4$ and with Lamé parameter λ and μ according to the elasticity modulus is $E = 10^5$ and the Poisson's ratio $\nu = 0.499$. The volume force and the traction boundary data vanish, and the Dirichlet boundary conditions are taken from the exact solution. The exact solution exhibits a strong singularity at the origin x_c .

The sequence of meshes is generated uniformly by the initial mesh from Figure 5.2. It is unnecessary to deal with the degrees of freedom at corner vertices due to the zero traction boundary data. However, considering the singularity of the exact solution at x_c , we would like to investigate the performance of the mixed FEM in [24] after relaxing the C^0 continuity at x_c as in Subsect. 4.1. Table 5.1 demonstrates that after the remedy, the errors of $\|\sigma - \sigma(\widetilde{\mathcal{T}})\|_A$ and $\|u - u(\widetilde{\mathcal{T}})\|_0$ are largely reduced. This is because the relaxation of the continuity at the origin x_c adds several more degrees of freedom at x_c .

5.3. Cook's membrane problem with treatment of corners on uniform meshes. The underlying domain is a quadrilateral with vertices at $(0, 0)$, $(48, 44)$, $(48, 60)$ and $(0, 44)$. It is fixed ($u = 0$) at the left edge of the boundary ($x_1 = 0$) while a uniform traction force pointing upwards ($\sigma n = (0, 1)^T$) is applied at the right edge ($x_1 = 48$). At the remaining part of the boundary it is kept in equilibrium ($\sigma n = 0$), see Figure 5.3. The elasticity

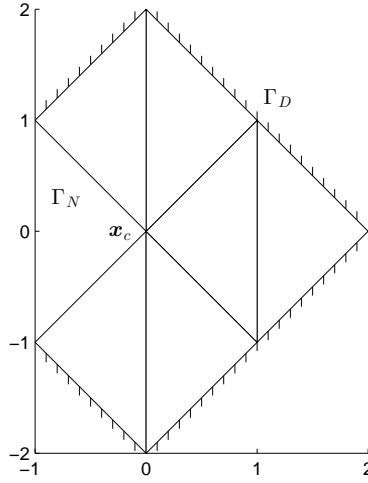


FIGURE 5.2. Initial mesh for the L-shaped domain

TABLE 5.1. A benchmark problem on L-shaped domain on uniform meshes

$\ \sigma - \sigma(\hat{\mathcal{T}})\ _A$			
Before remedy	Order	After remedy	Order
7.5143E-03		3.1046E-03	
5.5899E-03	0.4268	2.1945E-03	0.5005
3.9400E-03	0.5046	1.5147E-03	0.5348
2.7379E-03	0.5251	1.0416E-03	0.5402
1.8894E-03	0.5351	7.1517E-04	0.5424
$\ u - u(\hat{\mathcal{T}})\ _0$			
7.2407E-06		2.1190E-06	
3.8230E-06	0.9214	8.9234E-07	1.2477
1.8422E-06	1.0533	3.6866E-07	1.2753
8.8088E-07	1.0644	1.5774E-07	1.2247
4.1866E-07	1.0732	6.9708E-08	1.1782

modulus is $E = 10^5$ and the Poisson's ratio $\nu = 0.499$. At the corner nodes $\mathbf{x}_{c,1}$ and $\mathbf{x}_{c,2}$, there exist inconsistent traction boundary conditions.

This example relaxes the C^0 continuity at $\mathbf{x}_{c,1}$ and $\mathbf{x}_{c,2}$. Since the exact solution is unknown, the fine grid approximation is computed by the standard continuous P_5 -FEM on twice uniform refinements of the grid for the last level. Since the inconsistency of the boundary conditions at $\mathbf{x}_{c,1}$ and $\mathbf{x}_{c,2}$, the least squares method is employed before remedy to decide the values of stress at the two right corners. Table 5.2 shows that after the remedy, the errors are reduced, especially on coarse meshes. This happens because the error of inexact traction boundary conditions dominates on coarse meshes.

5.4. Cook's membrane problem with treatment of corners on adaptive meshes. In the case of $|\Gamma_N| \neq 0$ and $u_D \neq 0$ on Γ_D , the error estimator $\eta^2(\hat{\mathcal{T}})$ modifies $\mathcal{J}_{e,1}$ and $\mathcal{J}_{e,2}$ in

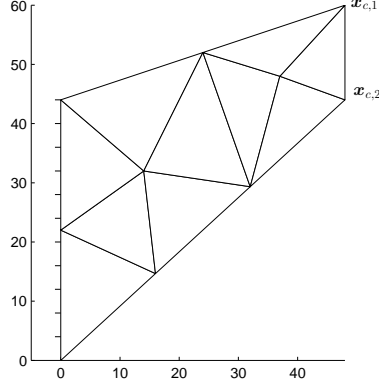


FIGURE 5.3. Initial mesh for Cook's membrane problem

TABLE 5.2. Cook's membrane problem on uniform meshes

$\ \sigma - \sigma(\hat{\mathcal{T}})\ _A$			
Before remedy	Order	After remedy	Order
0.0488		0.0341	
0.0299	0.7048	0.0241	0.5001
0.0190	0.6556	0.0167	0.5286
0.0121	0.6470	0.0113	0.5685
$\ u - u(\hat{\mathcal{T}})\ _0$			
6.2925E-03		2.1216E-03	
3.0423E-03	1.0485	1.0712E-03	0.9859
1.4886E-03	1.0311	5.3616E-04	0.9985
7.2422E-04	1.0395	2.7651E-04	0.9553

(3.5) from [18, Sec. 4] as follows

$$\mathcal{J}_{e,1} := \begin{cases} [(A\sigma(\hat{\mathcal{T}}))t_e \cdot t_e]_e & \text{if } e \in \hat{\mathcal{E}}(\Omega), \\ ((A\sigma(\hat{\mathcal{T}}))t_e \cdot t_e - \partial_{t_e}(u_D \cdot t_e))|_e & \text{if } e \in \hat{\mathcal{E}}(\Gamma_D), \end{cases}$$

$$\mathcal{J}_{e,2} := \begin{cases} [\text{curl}(A\sigma(\hat{\mathcal{T}})) \cdot t_e]_e & \text{if } e \in \hat{\mathcal{E}}(\Omega), \\ (\text{curl}(A\sigma(\hat{\mathcal{T}})) \cdot t_e + \partial_{t_e}(u_D \cdot n_e) - \partial_{t_e}((A\sigma(\hat{\mathcal{T}}))t_e \cdot n_e))|_e & \text{if } e \in \hat{\mathcal{E}}(\Gamma_D). \end{cases}$$

The reliability holds

$$\|\sigma - \sigma(\hat{\mathcal{T}})\|_A^2 \leq \widetilde{C}_{Rel}(\eta^2(\hat{\mathcal{T}}) + \text{osc}^2(f, \hat{\mathcal{T}}) + \text{osc}^2(g, \hat{\mathcal{E}}(\Gamma_N)))$$

with the data oscillation $\text{osc}^2(g, \hat{\mathcal{E}}(\Gamma_N)) := \sum_{e \in \hat{\mathcal{E}}(\Gamma_N)} h_e \|g - g(\hat{\mathcal{T}})\|_{0,e}^2$.

Define the total estimator $\eta := (\eta^2(\hat{\mathcal{T}}) + \text{osc}^2(f, \hat{\mathcal{T}}) + \text{osc}^2(g, \hat{\mathcal{E}}(\Gamma_N)))^{1/2}$. The discrete stress and the total estimator by the mixed FEM (2.8) before treatment is denoted by $\sigma(\hat{\mathcal{T}})^0$ and η^0 . The corresponding results after the relaxation of the C^0 continuity at $x_{c,1}$ and $x_{c,2}$ are denoted by $\sigma(\hat{\mathcal{T}})^M$ and η^M . The approximations by the standard continuous P_5 element on the very fine mesh are computed as the reference solutions. The results are shown in

Figure 5.4. Since the error of inexact boundary conditions dominates at the initial steps, the result without treatment is worse than that with treatment. After several refinements, the results are almost the same since the error of inexact boundary conditions has deduced greatly.

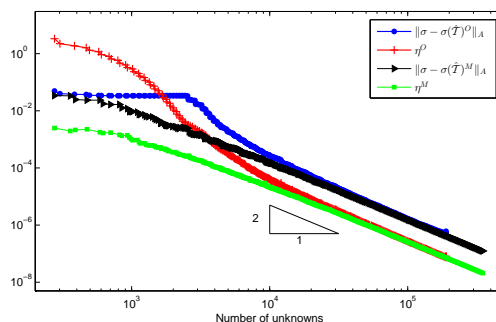


FIGURE 5.4. Errors $\|\sigma - \sigma(\hat{\mathcal{T}})\|_A$ and η vs #dofs for the Cook's membrane problem

5.5. Comparison of adaptivity algorithms for two mixed elements. This example compares the mixed element of $k = 3$ in [24] and the extended mixed element in Subsect. 3.1 for the benchmark problem over an L-shaped domain. The results are shown in Figure 5.5. Let $\sigma(\hat{\mathcal{T}})^O$ and η^O denote the discrete stress and the total estimator of the former element, and the corresponding results of the extended element by $\sigma(\hat{\mathcal{T}})^E$ and η^E . Figure 5.5 presents the convergence history plot and illustrates that there is not much difference between these two elements.

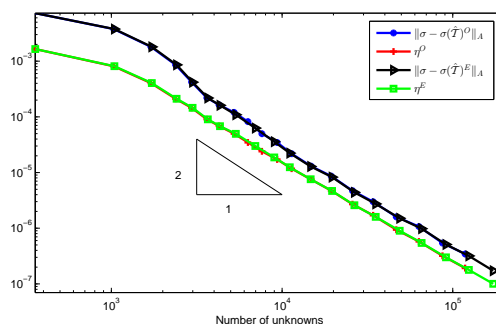


FIGURE 5.5. Errors $\|\sigma - \sigma(\hat{\mathcal{T}})\|_A$ and η vs #dofs for the problem on an L-shaped domain

REFERENCES

- [1] S. ADAMS AND B. COCKBURN, *A mixed finite element method for elasticity in three dimensions*, J. Sci. Comput., 25 (2005), pp. 515–521.
- [2] D. N. ARNOLD AND G. AWANOU, *Rectangular mixed finite elements for elasticity*, Math. Models Methods Appl. Sci., 15 (2005), pp. 1417–1429.
- [3] D. N. ARNOLD, G. AWANOU, AND R. WINTHER, *Finite elements for symmetric tensors in three dimensions*, Math. Comp., 77 (2008), pp. 1229–1251.
- [4] D. N. ARNOLD, F. BREZZI, AND J. DOUGLAS, *PEERS: A new mixed finite element for plane elasticity*, Jpn. J. Appl. Math., 1 (1984), 347–367, 1 (1984), pp. 347–367.

- [5] D. N. ARNOLD, R. FALK, AND R. WINTHER, *Mixed finite element methods for linear elasticity with weakly imposed symmetry*, Math. Comp., 76 (2007), pp. 1699–1723.
- [6] D. N. ARNOLD AND R. WINTHER, *Mixed finite element for elasticity*, Numer. Math., 92 (2002), pp. 401–419.
- [7] R. BECKER AND S. MAO, *An optimally convergent adaptive mixed finite element method*, Numer. Math., 111 (2008), pp. 35–54.
- [8] D. BOFFI, F. BREZZI, AND M. FORTIN, *Reduced symmetry elements in linear elasticity*, Commun. Pure Appl. Anal., 8 (2009), pp. 95–121.
- [9] D. BOFFI, F. BREZZI, AND M. FORTIN, *Mixed finite element methods and applications*, Springer, Heidelberg, 2013.
- [10] C. CARSTENSEN, M. FEISCHL, M. PAGE, AND D. PRAETORIUS, *Axioms of adaptivity*, Comput. Math. Appl., 67 (2014), pp. 1195–1253.
- [11] C. CARSTENSEN, D. GALLISTL, AND J. GEDICKE, *Residual-based a posteriori error analysis for symmetric mixed Arnold–Winther FEM*, Numer. Math., 142 (2019), pp. 205–234.
- [12] C. CARSTENSEN AND J. GEDICKE, *Robust residual-based a posteriori Arnold–Winther mixed finite element analysis in elasticity*, Comput. Methods Appl. Mech. Engrg., 300 (2016), pp. 245–264.
- [13] C. CARSTENSEN, D. GÜNTHER, J. REININGHAUS, AND J. THIELE., *The Arnold–Winther mixed FEM in linear elasticity. Part I: Implementation and numerical verification*, Comput. Methods Appl. Mech. Engrg., 197 (2008), pp. 3014–3023.
- [14] C. CARSTENSEN AND R. H. W. HOPPE, *Error reduction and convergence for an adaptive mixed finite element method*, Math. Comp., 75 (2006), pp. 1033–1042.
- [15] C. CARSTENSEN AND J. HU, *An extended Argyris finite element method with optimal standard adaptive and multigrid V-cycle algorithms*, preprint, (2019).
- [16] J. M. CASCON, C. KREUZER, R. H. NOCHETTO, AND K. G. SIEBERT, *Quasi-optimal convergence rate for an adaptive finite element method*, SIAM J. Numer. Anal., 46 (2008), pp. 2524–2550.
- [17] L. CHEN, M. HOLST, AND J. XU, *Convergence and optimality of adaptive mixed finite element methods*, Math. Comp., 78 (2009), pp. 35–53.
- [18] L. CHEN, J. HU, X. HUANG, AND H. MAN, *Residual-based a posteriori error estimates for symmetric conforming mixed finite elements for linear elasticity problems*, Sci. China Math., 61 (2018), pp. 973–992.
- [19] V. GIRAULT AND L. R. SCOTT, *Hermite interpolation of nonsmooth functions preserving boundary conditions*, Math. Comp., 71 (2002), pp. 1043–1074.
- [20] H. C. HU, *On some variational principles in the theory of elasticity and the theory of plasticity*, Acta Phys. Sin., 10 (1954), 259, pp. 259–290.
- [21] J. HU, *Finite element approximations of symmetric tensors on simplicial grids in \mathbb{R}^n : The higher order case*, J. Comput. Math., 33 (2015), pp. 283–296.
- [22] J. HU, *A new family of efficient conforming mixed finite elements on both rectangular and cuboid meshes for linear elasticity in the symmetric formulation*, SIAM J. Numer. Anal., 53 (2015), pp. 1438–1463.
- [23] J. HU AND G. YU, *A unified analysis of quasi-optimal convergence for adaptive mixed finite element methods*, SIAM J. Numer. Anal., 56 (2018), pp. 296–316.
- [24] J. HU AND S. ZHANG, *A family of conforming mixed finite elements for linear elasticity on triangular grids*, arXiv, 1406.7457 (2014).
- [25] J. HU AND S. ZHANG, *A family of symmetric mixed finite elements for linear elasticity on tetrahedral grids*, Sci. China Math., 58 (2015), pp. 297–307.
- [26] J. HU AND S. ZHANG, *Finite element approximations of symmetric tensors on simplicial grids in \mathbb{R}^n : The lower order case*, Math. Models Methods Appl. Sci., 26 (2016), pp. 1649–1669.
- [27] J. HUANG, X. HUANG, AND Y. XU, *Convergence of an adaptive mixed finite element method for Kirchhoff plate bending problems*, SIAM J. Numer. Anal., 49 (2011), pp. 574–607.
- [28] J. HUANG AND Y. XU, *Convergence and complexity of arbitrary order adaptive mixed element methods for the poisson equation*, Sci. China Math., 55 (2012), pp. 1083–1098.
- [29] C. JOHNSON AND B. MERCIER, *Some equilibrium finite element methods for two-dimensional elasticity problems*, Numer. Math., 30 (1978), pp. 103–116.
- [30] R. STEVENSON, *The completion of locally refined simplicial partitions created by bisection*, Math. Comp., 77 (2008), pp. 227–241.
- [31] X. ZHAO, J. HU, AND Z. SHI, *Convergence analysis of the adaptive finite element method with the red-green refinement*, Sci. China Math., 53 (2010), pp. 499–512.

LMAM AND SCHOOL OF MATHEMATICAL SCIENCES, PEKING UNIVERSITY, BEIJING 100871, P. R. CHINA. HUJUN@MATH.PKU.EDU.CN

LMAM AND SCHOOL OF MATHEMATICAL SCIENCES, PEKING UNIVERSITY, BEIJING 100871, P. R. CHINA. MARUIPKU@GMAIL.COM